Cilium proteomics reveals Numb as a positive regulator of the Hedgehog signaling pathway

Xiaoliang Liu[1,8], Patricia T. Yam[2,8], Wei-Ju Chen[2,5], Sabrina Schlienger[2,6], Oscar Torres Gutierrez[1], Eva Cai[1], Jingyi Zhang[1], Alice Y. Ting[3], Tess C. Branon[3,4], Michel Cayouette[2,6,7], Frédéric Charron[2,6,7*], Xuecai Ge[1*]

[1]Department of Molecular and Cell Biology, University of California, Merced, Merced California, 95340, USA.

[2]Montreal Clinical Research Institute (IRCM), Montreal, QC H2W 1R7, Canada.

[3]Departments of Genetics, of Biology, and by courtesy, of Chemistry, Stanford University, Stanford, California, USA. Chan Zuckerberg Biohub, San Francisco, California, USA.

[4]Current address: Interline Therapeutics, South San Francisco, CA, USA.

[5]Department of Biology, McGill University, Montreal QC H3A 0G4, Canada.

[6]Department of Anatomy and Cell Biology, McGill University, Montreal QC H3A 0G4, Canada.

[7]Department of Medicine, University of Montreal, Montreal QC H3T 1J4, Canada.

[8]These authors contributed equally.

*Correspondence: frederic.charron@ircm.qc.ca (F.C.), xge2@ucmerced.edu (X.G.)

Abstract

The transduction of Hedgehog (Hh) signaling relies on the primary cilium, a cell surface organelle acting as a signaling hub for the cell. Using proximity labeling and quantitative proteomics, we identified Numb as a new ciliary protein that positively regulates Hh signaling. Numb localizes to the ciliary pocket and acts as an endocytic adaptor to incorporate Ptch1 into clathrin-coated vesicles, thereby promoting Ptch1 exit from the cilium, a key step in Hh signaling activation. Numb loss impaired Sonic Hedgehog-induced Ptch1 departure from the cilium, resulting in severe attenuation of Hh signaling. Genetic ablation of *Numb* and its homolog *Numblike* in the developing cerebellum impaired the proliferation of granule cell precursors, a Hh-dependent process, resulting in reduced cerebellar size. This study demonstrates a key function of Numb in controlling protein levels in the cilium, and highlights Numb's critical role in the regulation of Hh signaling.

INTRODUCTION

The primary cilium acts as a cellular antenna that senses molecules and conveys their signal from the extracellular milieu into the cell (Eggenschwiler and Anderson, 2007; Goetz and Anderson, 2010). Hedgehog (Hh) signaling was the first signaling pathway discovered to rely on the primary cilium (Huangfu et al., 2003). Hh signal transduction is carried out by the dynamic transport of signal transducers into and out of the cilium. In the basal state, the Hh receptor Ptch1 resides in the cilium where it prevents the accumulation and activation of Smo in the cilium (Rohatgi et al., 2007). Upon binding to its ligand Shh, Ptch1 is inactivated and exits the cilium. Reciprocally, Smo is activated and accumulates in the cilium. Active Smo triggers a signaling cascade that eventually activates Gli transcription factors which then turn on the transcription of Hh target genes (Kim et al., 2009; Kong et al., 2019). During this process, Ptch1 exit from the cilium acts as a key step to initiate Hh signaling.

Recent studies suggest that Ptch1 acts as a sterol transporter to control local sterol components, such as cholesterols, in the cilium (Deshpande et al., 2019; Rudolf et al., 2019; Zhang et al., 2018). Binding to certain oxysterols is required for Smo activation (Huang et al., 2016; Raleigh et al., 2018). Therefore, Ptch1 is believed to inhibit Smo by restricting Smo's access to activating sterols in the ciliary membrane. The clearance of Ptch1 from the cilium correlates with Shh-mediated pathway activation and is necessary for maximal activation of Hh signaling (Kim et al., 2015; Rohatgi et al., 2007; Yue et al., 2014). However, the endocytic machinery that mediates Ptch1 exit from the cilium remains largely unknown. Two previous studies have reported mechanisms that regulate Ptch1 levels at the cytoplasmic membrane. Ptch1 was shown to be a substrate of the E3 ubiquitin ligases Smurf1 and Smurf2, and ubiquitination of Ptch1 promotes its lysosomal degradation (Yue et al., 2014). However, as this mechanism regulates cytoplasmic membrane levels of Ptch1 in the whole cell, whether it directly regulates Ptch1 exit from the cilium remains unknown. In non-canonical Shh signaling, endocytosis of Ptch1 in commissural neuron growth cones requires the endocytic adaptor protein Numb (Ferent et al., 2019). Numb mediates the internalization of Ptch1 and its co-receptor Boc into early endosomes of growth cones following Shh binding, and is required for non-canonical Hh signaling and growth cone turning up

Shh gradients. Whether Numb acts as an endocytic adaptor to mediate Ptch1 departure from the cilium in canonical Hh signaling remains to be determined.

A critical approach to understanding signaling mechanisms in the cilium is to catalog the dynamic protein components in the cilium in the course of signal transduction. This has been technically challenging due to the miniature size of the cilium, which accounts for about 1/10,000 of the cytoplasmic volume. Proximity-based labeling tools provide a powerful method to specifically label and identify ciliary proteins. APEX and its variant APEX2, engineered peroxidases, have been used to specifically label proteins in the cilium (Kohli et al., 2017; May et al., 2021; Mick et al., 2015). These enzymes were targeted to the primary cilia via distinct ciliary proteins. Intriguingly, when the enzyme was targeted to different sub-ciliary domains by fusing to distinct "tagging" proteins, unique cohorts of cilium proteins were discovered (Kohli et al., 2017; May et al., 2021; Mick et al., 2015).

In this study, we leveraged a mechanistically different proximity labeling tool, TurboID, to plot ciliary proteins in the course of Hh signal transduction. TurboID is an engineered promiscuous biotin ligase that labels neighboring proteins and avoids the need for toxic labelling conditions dependent on hydrogen peroxide (Branon et al., 2018). Using the membrane-associated ciliary protein Arl13b to tag TurboID, our ciliary proteome recovered many membrane-associated proteins and signal transducers. We identified Numb as a new ciliary protein. We showed that Numb localizes to the ciliary pocket, a cytoplasmic membrane region at the base of the cilium that "folds back" to ensheath the cilium. Moreover, we found that Numb interacts with Ptch1 and recruits Ptch1 to clathrin coated vesicles (CCVs), thereby promoting Ptch1 exit from the cilium. Numb loss reduces the intensity of Hh signaling in response to Shh in NIH3T3 cells and in granule cell precursors (GCPs). *In vivo*, genetic ablation of *Numb* in the developing cerebellum decreased the proliferation of GCPs, a Hh-signaling dependent process, resulting in a smaller cerebellum. Overall, our study highlights the profile of membrane-associated proteins and signal transducers in the cilium and demonstrates *in vitro* and *in vivo* the molecular role of Numb as a critical positive regulator of the Hh pathway and Hh-dependent developmental events.

RESULTS

Cilium-TurboID selectively biotinylates ciliary proteins

Many signaling proteins are membrane proteins or recruited to the membrane during signal transduction. To label these proteins in the primary cilium, we directed TurboID to the juxtamembrane region of the cilium. We chose Arl13b to fuse with TurboID since Arl13b is anchored to the ciliary membrane via lipid modification (Larkins et al., 2011; Roy et al., 2017), maximizing the chance of protein biotinylation in the juxtamembrane region. As reported before, overexpressing full length Arl13b leads to markedly elongated cilia in NIH3T3 cells (Lu et al., 2015a) (Fig. S1A). To determine which domains of Arl13b could retain ciliary localization without altering cilium length, we generated a series of truncated Arl13b constructs and transiently expressed them in NIH3T3 cells (Fig. 1A and Fig. S1A). We found that the N+RVEP+PR construct fits this requirement. This construct contains the N-terminal amphipathic helix (containing a palmitoylation modification for membrane association), the previously reported sequence RVEP

that is critical for cilium targeting, and the Proline Rich domain at the C-terminus (Nozaki et al., 2016) (Fig. 1A). In contrast, the construct containing only the PR domain showed no ciliary localization (Fig. S1A-B).

We next fused TurboID to N+RVEP+PR (cilium-TurboID), and to the PR domain (non-cilium-TurboID) as a control for cytosolic proteins. We then generated stable NIH3T3 cell lines that express cilium- or non-cilium-TurboID. To achieve physiologically relevant expression levels of the transgene, we used lentivirus with the UBC promoter to generate the stable cell lines. Confocal microscopy confirmed that cilium-TurboID is exclusively localized to the primary cilium, whereas non-cilium-TurboID is diffusely distributed in the cytoplasm (Fig. 1B). Furthermore, 10 min labeling with biotin selectively labeled proteins in the cilium in cilium-TurboID cells, whereas cytosolic proteins were labeled in non-cilium-TurboID cells (Fig. 1B).

To ensure that the transgenes did not impair cilium function, we measured cilium length and Hh signaling activity in the stable cell lines. We found that the cilium lengths are comparable between WT (parental NIH3T3 cells), cilium-TurboID and non-cilium-TurboID cells (Fig. S2A). We then determined the Hh signaling activity after the cells were stimulated with SAG, a Smo agonist. The Hh signaling activity was evaluated by the transcript levels of *Gli1*, a Hh target gene. We found that SAG-induced Gli1 levels were comparable between WT and stable cell lines (Fig. S2B). Further, SAG-induced cilium transport of Smo and Gli2 are indistinguishable between WT and the stable cell lines (Fig. S2C-S2F). In summary, the cilium morphology and Hh signaling are normal in these stable cell lines. Thus, we developed a method to exclusively target TurboID to the juxtamembrane microdomain in the primary cilium without impacting cilium functions.

Quantitative proteomics with cilium-TurboID highlighted membrane-associated ciliary proteins

We then employed the stable cell lines to label and isolate endogenous ciliary proteins. We labeled cells with biotin for 10 min and captured the biotinylated proteins with streptavidin beads (Branon et al., 2018). Proteins were analyzed by Western blotting (Fig. 2A). Streptavidin-HRP detection of the biotinylated proteins showed that biotin labeling drastically increased the amount of biotinylated proteins captured by the streptavidin beads. As a positive control, we examined PDGFRα, a receptor known to be localized to the cilium. As expected, PDGFRα was pulled down from cilium-TurboID cells, but not non-cilium-TurboID cells (Fig. 2A). These results confirm that cilium-TurboID is effective in labeling proteins in the cilium.

Next, we designed a quantitative proteomic experiment to capture the dynamic protein transport in the cilium in response to Shh stimulation. To control for background biotinylation, we included conditions that omitted either Shh stimulation or biotin labeling. To control for non-ciliary protein biotinylation by TurboID, we collected samples from stimulated and labeled non-cilium-TurboID cells (Fig. 2B). We prepared each condition with three independent replicates. After on-beads digestion, each sample was labeled with one channel of the 16plex TMT labeling kit. A reference channel was included in which equal volumes from each of the 12 samples were pooled. After that, the 13 samples were multiplexed and analyzed by liquid chromatography (UPLC)/MS-MS (Fig. 2B).

For data analysis, we defined the relative protein abundance as the ratio of normalized abundance in each channel over that in the reference channel. Only proteins with more than 7 unique peptides were used in data analysis. We determined candidate ciliary proteins via statistical analyses of the relative enrichment between the cilium-TurboID and the non-cilium-TurboID datasets. To be scored as ciliary proteins in the absence of Shh stimulation, candidates had to fulfill four criteria: 1) greater than 2-fold enrichment (TMT ratio > 2) in the labeled cilium-TurboID samples over the non-labeled cilium-TurboID samples, 2) and over the labeled non-cilium-TurboID samples; 3) statistically significant (p value < 0.05) enrichment in the labeled cilium-TurboID samples versus the non-labeled cilium-TurboID samples, and 4) versus the labeled non-cilium-TurboID samples (Fig. S3A-B). 788 proteins meet these criteria. To be scored as ciliary proteins after Shh stimulation, candidates had to fulfill the same four criteria, comparing between the labeled Shh-stimulated cilium-TurboID samples and the non-labeled Shh-stimulated cilium-TurboID samples, and the labeled Shh-stimulated non-cilium-TurboID samples (Fig. S3C-D). 574 proteins meet these criteria. Finally, we took the union of the above two categories and define these proteins as ciliary candidates regardless of Shh stimulation. We obtained 800 such ciliary candidates in total. A heatmap of each protein's relative abundance in the 12 samples demonstrated a high reproducibility across the triplicates (Fig. 2C).

We then compared the intensity of the above identified ciliary candidates between the Shh-stimulated and unstimulated conditions (Fig. 2D). We identified 30 proteins that show statistically significant changes (TMT ratio > 1.2 or < 0.83, p < 0.05). Among them is the Hh transducer Smo. It is important to note that lack of statistical significance does not imply that the candidates do not respond to Hh signaling, owing to a variety of reasons such as 1) the low abundance of the protein in the cilium, and 2) preferential biotinylation of proteins in juxtamembrane subdomain in our experimental settings. Indeed, a few proteins known to translocate to the cilium in response to Hh activation show larger p value, such as Gli2 and PALD1 (May et al., 2021).

Among the total ciliary candidates, 108 have been reported before to localize to the cilium (Fig. S3E). Analysis of the ciliary candidates with enrichment of Gene Ontology (GO) terms in Metascape shows that the largest cohort are membrane-associated proteins (Fig. 2E). These results validated our strategy of targeting TurboID to the ciliary juxtamembrane domain.

Numb localizes to the ciliary pocket and clathrin-coated vesicles (CCVs)

Among the newly identified ciliary candidates, one interesting protein is Numb. *Drosophila* Numb has important roles in asymmetric cell division (Roegiers and Jan, 2004), and mammalian Numb regulates neurogenesis in the developing brain (Li et al., 2003; Petersen et al., 2002; Zhong et al., 2000). However, the cilium localization of Numb has never been described before. Our proteomic results revealed Numb as a potential ciliary protein, and its intensities in the cilium show no significant changes when stimulated with Shh (Fig. 2D). To validate its ciliary localization, we expressed V5 tagged Numb in NIH3T3 cells. We found that in addition to its reported distribution in the cytosol as puncta (Abdi et al., 2019; Nishimura and Kaibuchi, 2007), Numb-V5 also overlaps with the ciliary marker Arl13b. However, the Numb immunofluorescence signal is

not distributed along the entire cilium; rather, it is restricted to the lower four-fifths of the cilium (Fig. S4A).

The localization pattern of Numb in the cilium does not resemble any of the known cilium subdomains, such as the transition zone (Reiter et al., 2012), Inversin zone (Shiba et al., 2009), or Evc zone (Dorn et al., 2012). Rather, it resembles the recently characterized ciliary pocket, a cytoplasmic membrane region at the bottom of the cilium that often folds back to ensheath the bottom of the primary cilium (Ghossoub et al., 2011; Molla-Herman et al., 2010). To characterize Numb's localization in the ciliary pocket, we co-transfected NIH3T3 cells with Numb-mCherry and EHD1-GFP, a protein known to localize to the ciliary pocket (Lu et al., 2015b) (Fig. 3A). We then performed expansion microscopy, a procedure that physically expands the samples in an isotropic fashion (Wassie et al., 2019), and we imaged the cells with an Airyscan confocal microscope, resulting in the resolution of structures beyond the diffraction limit of light. The cilium axoneme is highlighted with acetylated-tubulin staining. We found that Numb overlaps with EHD1 at the lower part of the cilium in the region flanking the cilium axoneme (Fig. 3A, A'), suggesting that Numb localizes to the ciliary pocket.

In addition to the ciliary pocket, Numb immunofluorescence appeared as discrete puncta in the cytosol (white triangles in Fig 3A). Since Numb is an adapter protein for clathrin-mediated endocytosis (Nishimura and Kaibuchi, 2007), these puncta are most likely clathrin-coated vesicles (CCVs). To test this, we co-transfected NIH3T3 cells with Numb-GFP and Clathrin-mCherry, and imaged cells after expansion microscopy. We found that at the bottom of the cilium, all Numb-containing puncta are clathrin positive, suggesting that these puncta are CCVs (Fig. 3B). Further, multiple double positive puncta are closely associated with the cilium (Fig. 3B, cyan triangles), indicating that these are CCVs or Clathrin-coated pits (CCPs) being formed from the ciliary pocket, as reported in previous studies (Milenkovic et al., 2009; Molla-Herman et al., 2010). Taken together, Numb localizes to the ciliary pocket and to CCVs derived from the ciliary pocket (Fig. 3C).

Numb interacts with Ptch1 and incorporates Ptch1 into CCVs

The ciliary pocket is a crucial site for endocytic control of ciliary proteins (Milenkovic et al., 2009; Molla-Herman et al., 2010). Meanwhile, our data show that Numb localizes to the ciliary pocket and to CCVs associated with the ciliary pocket. Therefore, it is possible that Numb functions as an endocytic adaptor for ciliary proteins. During Hh signal transduction, Ptch1 exit from the cilium is a critical step to ensure the maximal activation of Hh signaling (Yue et al., 2014). We hypothesized that Numb recruits Ptch1 to CCVs at the ciliary pocket, thereby mediating Ptch1 exit from the cilium.

To test our hypothesis, we first examined whether Ptch1 and Numb interact with each other in cells. In 293T cells, Ptch1-GFP co-immunoprecipitated with Numb-HA (Fig. 3D), suggesting that Ptch1 interacts with Numb. We then tested whether endogenous Ptch1 and Numb form complexes with each other in ciliated cells. We immunoprecipitated endogenous Numb from lysates of NIH3T3 cells and found that endogenous Ptch1 co-immunoprecipitated with Numb (Fig. 3E). In conclusion, Numb and Ptch1 form complexes with each other.

Next, we determined whether Ptch1 is incorporated into Numb-containing CCVs. We co-expressed Numb-mCherry and Ptch1-GFP in NIH3T3 cells via lentiviruses that allow low expression levels in order to recapitulate the behavior of endogenous proteins. To induce Ptch1 exit from the cilium, we stimulated cells with Shh for 30 min. Imaging from expansion microscopy showed that Ptch1-GFP overlaps with Numb-containing CCVs in the ciliary pocket and in the cytosol at the bottom of the cilium. Intriguingly, a brief stimulation with Shh markedly increased the percentage of Numb-containing CCVs that incorporates Ptch1-GFP (Fig. 3F-G), suggesting that Shh stimulation promotes Ptch1 internalization via Numb. Thus, Numb interacts with Ptch1 and might incorporate Ptch1 into CCVs to promote Ptch1 internalization from the ciliary pocket upon Shh stimulation.

Numb is required for Shh-induced Ptch1 exit from the cilium

To determine Numb's role in Ptch1 exit from the cilium, we generated Numb knockout cells via CRISPR/Cas9 in NIH3T3 cells. We used two guide RNAs to target the first and third exons of Numb, and isolated 14 single cell colonies of Numb knockout (KO) cells (Fig. S5A). We then validated biallelic indel mutations that eliminate Numb expression in two of the cell clones (Fig. S5B). Further, in these two clones, Numb protein was undetectable in Western blotting (Fig. 4A). We used these two cell clones in the subsequent experiments.

We next determined the impact of Numb loss on the exit of Ptch1 from the cilium. As reported before (Rohatgi et al., 2007), in unstimulated cells, Ptch1 in the cilium is below detection threshold of immunostaining, but overnight SAG treatment induces Ptch1 expression and localization to the cilium (Fig. 4B). Following that, Shh stimulation triggers Ptch1 exit from the cilium. In WT cells, only 56.7 ± 2.5% of Ptch1 intensity remained in the cilium after Shh stimulation for 1 hr. In contrast, in Numb KO cells, a significantly higher amount of Ptch1 remained in the cilium after Shh stimulation (73.2 ± 2.0% in Numb KO #1, 77.4 ± 1.6% in Numb KO #2) (Fig. 4B-C). Thus, Numb loss impedes Ptch1 exit from the cilium.

Numb is required for activation of Hh signaling

In the absence of Hh stimulation, Ptch1 in the cilium suppresses Smo activation (Fig. 5A). Hh stimulation induces Ptch1 exit from the cilium, which is critical for the activation of Hh signaling. We predicted that without Numb, Hh signaling would be suppressed due to impaired Ptch1 exit from the cilium. To test this, we evaluated Shh-induced Hh signaling in Numb CRISPR/Cas9 KO cells. We stimulated cells with Shh and assessed Hh signaling activity by measuring the transcript levels of the Hh target genes, *Gli1* and *Ptch1*. As predicted, Numb loss severely attenuated Shh-induced transcription of Hh target genes, especially at the higher doses of Shh (Fig. 5B-C). We further confirmed this with an alternative method to silence Numb expression. We infected cells with lentiviruses that express Numb shRNA (Fig. S6A) and stimulated cells with the highest dose of Shh. Two independent shRNA constructs against Numb attenuated Shh-induced *Gli1* and *Ptch1* transcription to the same extent as Numb CRISPR/Cas9 mediated KO (Fig. S6B-C).

Consistent with our quantitative PCR experiments, we found that Numb loss significantly reduced Gli1 protein levels (Fig. 5D-E), most likely as a consequence of attenuated *Gli1* transcription. Thus, Numb loss impaired Hh signaling activation.

To exclude potential off-target effects of CRISPR/Cas9, we infected the Numb KO cells with lentiviruses that express Numb-V5. As expected, restoring Numb expression in Numb KO cells rescued Shh-induced *Gli1* transcription (Fig. 5F). As Numb regulates Hh signaling at the level of Ptch1, we predict that activating the pathway downstream of Ptch1 should rescue Hh signaling in Numb KO cells. Hence, we expressed SmoM2, a constitutively active Smo (Xie et al., 1998), in Numb KO cells. We found that SmoM2 expression activates Hh signaling in Numb KO cells to levels comparable to WT cells (Fig. 5G). Thus, consistent with its roles in controlling Ptch1 exit from the cilium, Numb acts to regulate Hh signaling upstream of Smo.

We also recovered Numb's homolog Numblike (Numbl) in our cilium proteomics (Fig. 2C). Although no studies implicate Numbl in endocytosis, in some contexts, such as neurogenesis in the cerebral cortex, Numbl plays redundant roles with Numb (Li et al., 2003; Petersen et al., 2002; Zhong et al., 2000). Hence, we characterized the localization of Numbl and its function in Hh signaling. Similarly to Numb, Numbl-V5 localizes to the bottom four-fifths of the primary cilium. However, unlike Numb, Numbl does not appear as discrete puncta in the cytosol (Fig. S4B), suggesting that Numbl may not act as an endocytic adapter. We then determined whether Numbl is required for Hh signal transduction. We silenced Numbl with shRNA (Fig. S7A) and found that it does not impact Shh-induced Hh target gene transcription (Fig. S7B). Further, silencing Numbl in Numb KO cells does not further reduce Shh-induced Hh target gene transcription (Fig. S7B). Therefore, Numbl is not essential for Hh signaling transduction.

Numb is expressed in GCPs and is required for Shh-induced GCP proliferation

During development, canonical Hh signaling regulates cell fate specification and proliferation. In particular, during cerebellum development, Shh secreted by Purkinje cells activates Hh signaling in GCPs and drives their proliferation in the external granule layer (EGL) from E17.5 until early postnatal development (Dahmane and Ruiz-i-Altaba, 1999; Wallace, 1999; Wechsler-Reya and Scott, 1999). Given the requirement for Numb in Hh signal transduction in NIH 3T3 cells (Fig. 5), we hypothesized that Numb may also be required for Hh signaling in GCPs.

RNA sequencing of isolated mouse postnatal day 7 (P7) GCPs confirmed that *Numb* transcript is present in GCPs (Tamayo-Orrego et al., 2020). To test whether Numb is required for Hh signaling in GCPs, we first assessed the effect of Numb loss in GCPs on the expression of the Hh target gene *Gli1*. Although our results in NIH3T3 cells indicate that Numbl is not involved in Hh transduction, Numbl was shown to compensate for Numb loss in the developing brain (Li et al., 2003; Petersen et al., 2002). Hence, to avoid any potential compensation from Numbl when we examined Numb's function in the developing cerebellum, we used mice null for *Numbl* (Bélanger et al., 2017) with *Numb* floxed alleles (Wilson et al., 2007), and crossed them with mice expressing Cre recombinase under the *Math1*-promoter (Matei et al., 2005). Expression of Math1-Cre conditionally removes *Numb* from GCPs. We then isolated and cultured GCPs from the cerebella of P7 *Math1-cre*$^{-}$*;Numb*$^{f/f}$*;Numbl*$^{-/-}$ and *Math1-cre*$^{+}$*;Numb*$^{f/f}$*;Numbl*$^{-/-}$ mice. Shh-induced *Gli1*

expression was measured by qRT-PCR. We found that when Numb is present, Shh markedly induced *Gli1* transcription, whereas removal of Numb significantly reduced Shh-induced Gli expression. This result demonstrates that Numb is required for maximal levels of Hh signaling in GCPs (Fig. 6A).

Next, we determined whether the reduced Hh signaling in GCPs lacking *Numb* and *Numbl* corresponded with a change in their proliferative response to Shh. We generated control mice (control) and mice conditionally lacking *Numb* and *Numbl* (*Numb;Numbl* cDKO). We isolated GCPs and determined Numb expression with Western blotting using an antibody that recognizes both Numb and Numbl (Kechad et al., 2012). We found that while Numb is expressed in GCPs from control cerebella, its expression is almost completely ablated in GCPs isolated from *Numb;Numbl* cDKO mice (Fig. 6B). This result confirms that *Math1-cre* efficiently removed *Numb* from GCPs.

Stimulation of control GCPs with Shh for 48 h induced their proliferation in a dose-dependent manner, as measured by ^{3}H-thymidine incorporation. *Numb;Numbl* cDKO GCPs had a significantly lower proliferative response to Shh (Fig. 6C), demonstrating that Numb is a positive regulator of the proliferative response to Shh. In contrast, *Numb;Numbl* cDKO GCPs had the same proliferative response as control GCPs to the Smo agonist purmorphamine (Fig. 6D), indicating that activating Smo induces cell proliferation independently of Numb/Numbl. Therefore, Numb acts at or above Smo in Shh-mediated GCP proliferation, consistent with its role in regulating Hh signaling at the level of Ptch1 (Fig. 5).

***Numb/Numbl* cDKO mice have reduced proliferation in the EGL of the cerebellum**

We next examined if the reduced GCP proliferation in response to Shh *in vitro* correlated with reduced proliferation *in vivo* in the cerebellum. Our immunostaining results show that Numb is expressed in the EGL of the cerebellum where GCPs are located (Fig. 7A), consistent with previous immunostaining results (Zhou et al., 2011) and *in situ* hybridization results and (Stump et al., 2002) (Fig. S8). *Numb;Numbl* cDKO cerebellum have significantly lower Numb immunostaining fluorescence intensity in the EGL (Fig. 7A-B), reflecting conditional removal of *Numb*.

We then used the mitotic marker phosphohistone H3 (pH3) to measure the number of proliferating cells in the EGL. We found that the EGL of *Numb;Numbl* cDKO cerebellum contains significantly fewer proliferating cells compared to the EGL of control mice (Fig. 7C-E). Thus losing *Numb;Numbl* reduces the number of proliferating GCPs *in vivo*.

To gain insights into the reduced GCP proliferation, we measured the length of the cell cycle in GCPs by sequential labeling with the thymidine analogs BrdU and EdU (Das et al., 2009). BrdU was administered to P6 pups for 2 h to label cells in S phase, followed by EdU for another 30 min, after which mice were euthanized for immunostaining. BrdU+ EdU- cells represent cells which were in S phase during the initial 2 h but exited S phase during the last 30 min. The length of cell cycle was calculated by: 2h x (PCNA^{+} cells/BrdU^{+}EdU^{-} cells). We found that GCPs in *Numb;Numbl* cDKO mice exhibit a longer cell cycle than GCPs in control mice (Fig. 7F-G),

consistent with their reduced proliferation. Taken together, our data suggest that Numb/Numbl is required for the Shh-induced GCP proliferation in the developing cerebellum.

Numb/Numbl cDKO mice have a smaller GCP population and cerebellar size

We anticipate that reduced GCP proliferation would lead to a smaller GCP population and fewer granule neurons, which usually leads to a reduction in the size of the cerebellum. To test this, we measured the area of the EGL, which is proportional to the size of the GCP population, and the overall cerebellar area in the developing cerebellum. We performed the measurement on sagittal sections from P6 cerebellum at the same mediolateral level. We found that both the EGL area and the overall cerebellar area were significantly smaller in *Numb;Numbl* cDKO mice compared to control mice (Fig. 8A-C).

After their proliferative phase, GCPs differentiate into mature granule neurons, exit the EGL and migrate inwards to populate the internal granule layer (IGL). To determine whether the reduced GCP proliferation leads to a smaller IGL, we measured the area of the IGL in cerebellar sections at the same mediolateral levels in adult mice. We found that the IGL area in *Numb;Numbl* cDKO mice is significantly smaller compared to that in control mice. Furthermore, the total area of the cerebellum in adult mice was also significantly smaller in *Numb;Numbl* cDKO mice compared to control mice (Fig. 8D-F). Although the IGL surface area was diminished, the organization of granule neurons did not appear to be affected. Taken together, these results demonstrate that the reduction in GCP proliferation and cerebellar size observed at P6 is not simply a delay in development. Finally, the total body weight of adult *Numb;Numbl* cDKO mice is comparable to that of control mice (Fig. 8G), indicating that the reduced cerebellar size is not due to an overall decrease in the body size of the *Numb;Numbl* cDKO mice.

In summary, Hh signaling activity is impaired in GCPs of *Numb;Numbl* cDKO mice, leading to reduced GCP proliferation. The reduction in GCP proliferation leads to a smaller EGL and IGL and a reduction in the overall size of the cerebellum. Thus, Numb positively regulates Hh signaling in GCPs and is required for GCP proliferation during cerebellar development.

DISCUSSION

In this study, we define Numb's role in Hh signal transduction and Hh-dependent cell proliferation. We found that Numb is required for Hh-induced Ptch1 exit from the cilium, a key step in the activation of Hh signaling (Fig. 8H). We show that Numb resides in the ciliary pocket. Given its function as an endocytic adaptor protein, we propose that Numb, through its ability to interact with Ptch1, recruits Ptch1 into CCVs thereby mediating Ptch1 internalization and exit from the cilium. In the absence of Hh stimulation, there are basal levels of Ptch1 internalization. Binding of Shh to Ptch1 increases Numb-mediated Ptch1 internalization, leading to Ptch1 exit from the cilium. This is essential for maximal intensity of the downstream signaling cascade that eventually turns on Hh-target gene transcription. In the absence of Numb, Ptch1 remains in the cilium even after binding to Shh, preventing the initiation of downstream Hh signaling (Fig. 8H). Indeed, in both NIH3T3 cells (Fig. 5) and GCPs (Fig. 6A), inactivating Numb resulted in an attenuation of Hh target gene expression. Moreover, in GCPs, inactivating Numb also resulted in an attenuation of

Shh-induced cell proliferation (Fig. 6C). Therefore, Numb is a positive regulator of Hh-signaling and Hh-dependent cell proliferation.

Cilium proteomics with TurboID revealed distinct groups of cilium proteins involved in Shh signaling

In this study, we leveraged TurboID, an engineered biotin ligase, to profile ciliary proteins. We recovered 108 known cilium proteins, including proteins that are well characterized to translocate to the cilium upon Hh activation, such as Smo and Pald1 (Corbit et al., 2005; May et al., 2021). Our results reveal a distinct group of cilium proteins, and only slightly overlap with results from previous cilium proteomic studies using APEX (Kohli et al., 2017; May et al., 2021; Mick et al., 2015). We captured a large percentage of membrane-associated proteins, whereas previous studies recovered high numbers of ciliary trafficking (IFTs and BBSome) proteins or actin binding proteins. We obtained a unique cohort of ciliary proteins with high potential for being signal transducers for the following reasons:

First, the distinct labeling mechanisms of TurboID and APEX allow them to label different protein substrates. TurboID, originally derived from the biotin ligase BirA (Roux et al., 2012), mediates biotin tagging to primary amines, such as the lysine sidechain of target proteins; in contrast, APEX is a derivative of ascorbate peroxidase that catalyzes the tagging of biotin-phenol to electron-dense residues such as tyrosine (Hung et al., 2016). APEX and BioID (another derivative of BirA) have been used in parallel to profile the ribosome quality control pathway, and the results showed minimal overlap between each other (Zuzow et al., 2018). Thus, different proximity labeling tools can target different cohorts of proteins. Second, the ciliary cytoplasm (~0.5 μm x 5 μm) is spacious compared to the labeling radius of TurboID and APEX (10-15 nm). Therefore, when the proximity labeling enzyme is tethered to discrete microdomains in the cilium, different proteins are labeled. We aimed to sample a different compartment of the cilium and potentially capture novel signal transducers in the cilium. For this, we tethered TurboID to the ciliary juxtamembrane domain via Arl13b, a lipid-linked membrane-associated protein. Arl13b has known functional interactions with Hh signaling components. These factors maximized our chance of capturing signal transducers that are recruited to the juxtamembrane region during signaling transduction. Finally, we leveraged NIH3T3 cells, a cell line that contains all the Hh pathway components and faithfully recapitulates the Hh signaling cascade.

Numb localizes to the ciliary pocket

The ciliary pocket refers to the invaginated cytoplasmic membrane at the bottom of the cilium that ensheathes part of the cilium axoneme. Although the function of the ciliary pocket remains largely mysterious so far, accumulating evidence suggests that it could be a crucial site for endocytosis of ciliary proteins (Ghossoub et al., 2011; Molla-Herman et al., 2010; Rohatgi and Snell, 2010). We used expansion microscopy and Airyscan confocal imaging to show that Numb localizes to the ciliary pocket (Fig. 3). However, immunostaining with an anti-Numb antibody failed to detect endogenous Numb in the ciliary pocket. This could be explained by low levels of Numb in the ciliary pocket and/or lack of sensitivity of the Numb antibody to low Numb levels. As an endocytic adaptor protein, Numb's localization to the ciliary pocket is transient, which might keep its local levels below the detection threshold of the Numb antibody. The same phenomenon has been

observed with other ciliary proteins, such as PKA. Multiple PKA subunits have been detected in the cilium by mass spectrometry (Mick et al., 2015). When fused to EGFP, PKA subunits were found in the cilium (Arveseth et al., 2021). However, immunostaining with PKA antibodies failed to detect endogenous PKA in the cilium. Overall, our results revealed a new role of Numb as an endocytic adaptor protein in the ciliary pocket.

Numb positively regulates Hh signaling

We found that Numb interacts with Ptch1 and is required for Hh-induced Ptch1 exit from the cilium (Fig. 4), thereby positively regulating Hh signaling. Without Numb, Ptch1 remains in the cilium even after binding to Shh, preventing the initiation of downstream Hh signaling (Fig. 8H). In both NIH3T3 cells (Fig. 5) and GCPs (Fig. 6A), inactivating Numb resulted in an attenuation of Hh target gene expression. Moreover, we were able to rescue the Hh signaling defects in Numb KO cells by: 1) restoring Numb expression (Fig. 5F), 2) expressing a constitutively active Smo mutant (Fig. 5F), and 3) stimulating the cells with a Smo agonist (Fig. 6D).

Our results differ from a previous report showing that Numb negatively regulates Hh signaling by facilitating the degradation of Gli1 (Marcotullio et al., 2006). Multiple lines of evidence support the idea that our results reveal the physiological role of Numb in Hh signaling. First, most experiments in Marcotullio et al. were conducted in non-ciliated cell lines, and hence may not be relevant to the physiological process of Hh signal transduction in the vertebrate system. Second, we rescued Hh signaling defects in Numb KO cells by expressing constitutively active Smo (SmoM2) or by stimulating cells with a Smo agonist (Fig. 5G and 6D). These results show that Numb regulates Hh signaling upstream of Smo, consistent with our identified roles of Numb in Ptch1 internalization from the ciliary pocket. Thus, our work demonstrates a positive role of Numb in Hh signaling. While our results do not rule out the possibility that Numb might also act negatively on the Gli1 protein by causing its degradation (Marcotullio et al., 2006), we found that – ultimately – ablation of Numb severely reduced Gli1 protein levels (Fig. 5D-E). This is most likely a consequence of the reduced *Gli1* transcription that we observed when Numb is removed, both in NIH3T3 and in GCPs. Moreover, the impact of genetically inactivating Numb *in vivo* is a decrease in Hh signaling, leading to reduced GCP proliferation and a smaller cerebellum. Thus, the positive role of Numb on the Hh pathway that we found is clearly dominant over its negative role.

Our discovery in NIH3T3 cells showing that Numb is a positive regulator of Hh signaling is supported by our analysis of *Numb;Numbl* cDKO mice. GCP proliferation, a Hh-dependent process, is markedly reduced in *Numb;Numbl* cDKO mice, leading to a reduction in EGL area (IGL in adult cerebellum) and a reduction in the overall size of the cerebellum. Numb has multiple functions in the nervous system, and has been implicated in various processes, including asymmetric cell division, cell fate determination, neurogenesis and cell migration (Yap and Winckler, 2015). In the developing cerebellum, Numb regulates granule cell maturation and Purkinje cell maturation (Klein et al., 2004) and is required for BDNF-mediated migration of GCPs after they exit the cell cycle (Zhou et al., 2011). Consistent with a role for Numb in granule cell maturation and proliferation, conditional removal of *Numb* with *En2-Cre*, a Cre line that ablates Numb from the entire hindbrain at early developmental stages, results in a smaller cerebellum (Klein et al., 2004).

Our results that Ptch1 clearance from the cilium is required for the maximal activation of Hh signaling is consistent with a previous report (Yue et al., 2014). In this study, the authors showed that Ptch1 turnover rate was controlled by Smurf-mediated ubiquitination and the ensuing degradation in the endosome. In Smurf-inactivated cells, Ptch1 levels in the cilia remain high after Shh stimulation, leading to attenuated Hh signaling and reduced GCP proliferation *in vitro*. Since Smurf is not known to localize to the cilium, the Smurf-mediated Ptch1 turnover of the overall Ptch1 levels in the cytoplasmic membrane might indirectly impacts Ptch1 levels in the cilium. In addition, it is unknown whether this role of Smurf occurs *in vivo*. Nonetheless, this mechanism may work in parallel to our model of Numb-mediated Ptch1 exit from the cilium: Numb functions in the endocytic machinery to mediate Ptch1 clearance from the cilium, and the destiny of endocytosed Ptch1 is determined by its ubiquitination status. Together, results from the study of Yue et al. and ours highlight the importance of Ptch1 clearance from the cilia in Hh signaling and GCP proliferation. Our discovery of Numb as a positive regulator of Hh signaling expands our understanding of Hh signaling and suggests that Numb may also regulate other Hh-dependent developmental processes.

ACKNOWLEDGEMENTS

We thank Dr. Rajat Rohatgi (Stanford University) for the gifts of CRISPR/Cas9 reagents, and Dr. Matthew Scott lab for the antibodies against Ptch1 and Smo. We thank Dr. David Gravano (Stem Cell Instrumentation Foundry, University of California, Merced) for fluorescence-activated cell sorting, and Dr. David Ardell (University of California, Merced) for consultation of proteomic data analysis. We thank Dr. Christopher J. Westlake (Center for Cancer Research, National Cancer Institute) for the gift of EHD1-GFP plasmid. We thank Francois Depault, Christine Jolicoeur and Jessica Barthe for expert technical assistance. We thank Julien Ferent for critical discussions. The data in this work was collected, in part, with a confocal microscope acquired through the National Science Foundation MRI Award Number DMR-1625733. Mass spectrometry was performed in the Vincent Coates Foundation Mass Spectrometry Laboratory, Stanford University Mass Spectrometry (RRID:SCR_017801) by Dr. Ryan Leib, Dr. Fang Liu, Kratika Singhal, and Rowan Matney. Research in the laboratory of X.G. was supported by NIH/NCI R15 (CA235749), NIH R01 (GM143276), UC CRCC seed grant (C21CR2007), and NSF CAREER award (IOS-2143711). Research in the laboratory of F.C. was supported by the Canadian Institutes of Health Research (FDN334023 and PJT471325), Brain Canada-Weston Foundation (to F.C. and M.C.), and the Canada Foundation for Innovation (33768). F.C. holds the Canada Research Chair in Developmental Neurobiology.

The authors declare no competing financial interests.

AUTHOR CONTRIBUTIONS

X. Ge, X. Liu, P.T. Yam and F. Charron conceived the project. X. Ge and X. Liu designed the experiments on cilium proteomics and Numb mechanistic study in cultured cells. X. Liu performed the experiments, analyzed, and interpreted the data on cilium proteomics and Numb study in

cultured cells. E. Cai curated and characterized the Numb CRISPR/Cas9 knockout cell lines. O. T. Gutierrez and J. Zhang performed experiments related to quantifications in the cilium length and cilium protein levels. P. T. Yam, W.J. Chen, S. Schlienger, M. Cayouette and F. Charron designed and performed the experiments on *numb;numbl* knockout mice, and analyzed and interpreted the data on cerebellar development and GCP proliferation. T. Branon and A. Ting provided the reagents for TurboID and provided technical support for TurboID related proteomics. X. Ge, X. Liu, P. T. Yam and F. Charron wrote the paper.

MATERIALS AND METHODS

Cell line generation, cultivation, and manipulation

NIH3T3 cells were cultured in DMEM (supplemented with 10% calf serum). Ciliation was induced by reducing the growth media to 0.5% CS for 24 h. Transfections were performed using Lipofectamine 2000 (Invitrogen) according to manufacturer's guidelines. *Numb* gene was disrupted in NIH3T3 cells using CRISPR/Cas9-mediated genome editing with gRNAs targeting exon 1. Clones of cell line were obtained by single-cell sorting. Clones with the disrupted gene were screened by immunofluorescence (IF) and Western blotting for the target protein using protein-specific antibodies. Selected positive clones were further characterized by sequencing, confirming missense mutation leading to early termination of translation and frameshift mutation. NIH3T3 cell lines stably expressing Cilium-TurboID and Non-cilium-TurboID were generated using lentivirus plasmids encoding Cilium-TurboID and Non-cilium-TurboID and confirmed by sequencing. To induce Shh signaling, growth media were supplemented with either 100 nM SAG or ShhN conditioned medium (20-30% [vol/vol] depending on batch) produced with 293 EcR-Shh-N cells.

TurboID labeling experiments and subcellular fractionation

Biotin labeling experiments were performed as described[24]. Briefly, cells were incubated in the presence of 50 μM biotin for 10 min. For non-labelled samples, water was added instead of biotin. After 10 min of incubation at 37℃, the medium was aspirated quickly, and cells were washed three times with 1× PBS. For fluorescence microscopy, cells were immediately fixed. For proteomic and Western blot analyses, cells were lysed with subcellular fractionation buffer (20 mM HEPES, 10 mM KCl, 2 mM MgCl2, 1 mM EDTA, 1 mM EGTA, 1mM DTT, pH 7.5 and protease inhibitors) and by 15 passages through a 27-G needle. Nuclei were separated from the post-nuclear supernatant (PNS) by centrifugation at 720 x g (3,000 rpm) for 5 min The PNS was also respun at 8,000 rpm (10,000 x g) for 5 min and then brought to Lysis Buffer (0.5% NP-40, 0.1% SDS, 0.5% sodium deoxycholate, 150 mM NaCl, 25 mM Tris/HCl, pH 7.5, and protease inhibitors), sonicated and clarified by centrifugation at 10,000g for 10 min.

Streptavidin capture

After determining the protein concentrations of lysates from the TurboID labeling experiments, they were adjusted to equal concentrations and volumes as starting material, from which samples were taken as loading control for SDS-PAGE and Western blot analysis. The remaining lysates were added onto washed and equilibrated streptavidin magnetic beads, and biotinylated proteins were allowed to bind for 1.5 h at room temperature. Beads with bound proteins were washed

extensively with a series of buffers to remove nonspecific binders: twice with Lysis Buffer, once with 1 M KCl, once with 0.1 M Na2CO3, once with 2 M Urea in 10 mM Tris-HCl, pH 8.0, twice with Lysis Buffer, and finally with 1 x PBS. For Western blot analysis, the beads were eluted with 2 x SDS sample buffer.

On-beads trypsin digestion of biotinylated proteins and TMT labeling

Beads with bound proteins were incubated in 100 mM TEAB and reduced using 10 mM DTT at 55°C for five minutes, followed by 25 minutes at room temperature with head-over-head mixing. The reduced proteins were alkylated using 30 mM acrylamide for an additional 30 minutes of room temperature with head-over-head mixing. Peptides were digested using trypsin/LysC (Promega) overnight with head-over-head mixing. Peptides were quenched with 1% formic acid and separated from the beads; 0.1% formic acid was used as a second elution prior to C18 microspin column clean up and speedvac to dryness. Peptides were quantified using the Pierce Quantitative Fluorometric Peptide Assay (Thermo) to match input peptide amounts for TMT labeling. Aliquots of each sample were pooled for a common reference prior to isobaric labeling. Peptides were resuspended in 100 mM TEAB and tagged as described in the manufacturer's protocol. Tagged peptides were then pooled to generate a multiplexed sample. This sample was then fractionated offline using high pH reverse-phase fractionation to increase peptide observations.

Mass spectrometry

In a typical mass spectrometry (MS) experiment, dried, desalted, labeled peptides were reconstituted in 2% aqueous acetonitrile. MS experiments were performed using liquid chromatography (LC) with an Acquity M-Class UPLC (Waters) followed by MS using an Orbitrap Fusion Tribrid MS (Thermo Scientific). A flow rate of 300 nL/min was used, where mobile phase A was 0.2% (v/v) aqueous formic acid and mobile phase B was 0.2% (v/v) formic acid in acetonitrile. Analytical columns were prepared in-house, with an internal diameter of 100 µm packed with NanoLCMS solutions 1.9 um C18 stationary phase to a length of approximately 25 cm. Peptides were directly injected into the analytical column using a gradient (2% to 45% B, followed by a high-B wash) of 120 min for each fraction. MS was operated in a data-dependent fashion using Collision-Induced Dissociation (CID) fragmentation for MS/MS spectra generation collected in the ion trap on the Fusion with MS3 detection of the reporter ions using synchronous precursor selection (SPS) to improve measuring accuracy as described previously (Li et al., 2020).

MS Data Analysis

For data analysis, the .RAW data files were checked using Preview (Protein Metrics) to verify calibration and quality prior to further analysis. Data were then processed using Proteome Discoverer v1.5 (Thermo) for quantitative analysis of reporter ion ratios, and using the Byonic (Protein Metrics) node to identify peptides and infer proteins against the *Mus musculus* database from Uniprot (including isoforms and concatenated with common contaminant proteins). Proteolysis with Trypsin/LysC was assumed to be specific with up to two missed cleavage sites, and allowing for common modifications. Precursor mass accuracies were held within 12 ppm with

fragment ions held within 0.4 Da (for CID) and 12 ppm (for HCD). Proteins were held to a false discovery rate of 1%, using standard approaches described previously (Elias and Gygi, 2007).

Quantitative real-time PCR

NIH 3T3 cells were grown in 24-well plates in regular growth medium for 24 h, followed by serum starvation to induce ciliation and addition of SAG or Shh-N conditioned (or control) medium to induce Shh signaling. After 24 h, cells were RNA extracted using Trizol reagent (Invitrogen). Quantitative PCR was performed on 100 ng total RNA per reaction using Quantstudio 3 System (Applied Biosystems) and qPCR reagents (QuantaBio; qScript XLT One-Step RT-qPCR ToughMix, Low ROX). The TaqMan gene expression probes used were Mm00477927_m1 (*Numb*), Mm00477931_m1 (*Numblike*), Mm00494645_m1 (*Gli1*), Mm00436026_m1 (*Ptch1*) and Mm99999915_g1 and *GAPDH* to normalize the samples.

P6 GCPs were seeded at $2.5x10^6$ cells/well in 6-well plates. GCP cells were treated or not with 1 nM recombinant ShhN for 20 h and pellets were directly resuspended in the lysis buffer. RNA was purified using the RNeasy Mini Plus kit (QIAGEN). cDNA was synthesized using the Transcriptor First Strand cDNA synthesis kit (Roche) using total RNA. Real-time PCR mixes were prepared using Perfecta SYBR Green Supermix (Quanta Biosciences). Reactions were performed in triplicate, and the amount of cDNA per reaction was 5 ng. Results were analyzed using the Comparative Ct method. The levels of *Gli1* mRNA were normalized to *Gusb* mRNA. The primers used were *Gli1* F: GCA GTG GGT AAC ATG AGT GTC T and *Gli1* R: AGG CAC TAG AGT TGA GGA ATT GT.

Immunofluorescence and microscopy

Cells were grown on round 12 mm #1.5 coverslips and fixed in 4% PFA for 10–15 min at room temperature. After fixation, cells were permeabilized and blocked in blocking buffer (2% donkey serum, 0.2% triton X-100, in PBS) for 1 h at room temperature. After blocking, cells were incubated with primary antibody diluted in blocking buffer for 1 h at room temperature or 4°C overnight, washed three times with 1× PBS over 15 min, and incubated with Alexa Fluor 488-, rhodamine-, or Alexa Fluor 647-coupled secondary antibodies (Jackson ImmunoResearch) in blocking buffer for 1 h, and then incubated in Hoechst (1ug/ml in PBS) for 10 min. Finally, cells were washed five times in PBS and mounted on glass slides using Fluoromount G (Southern Biotech; 0100-01). Prepared specimens were imaged on a Leica DMi8 (LAS X software) with Plan Apochromat oil objectives (63x, 1.4 NA) or a LSM880 confocal microscope (Zeiss). Images were processed using ImageJ.

Expansion microscopy

The gelation and proteinase digestion steps are similar to the proExM protocol (Tillberg et al., 2016) with two modifications: (1) after cells are fixed and stained with primary antibodies, we added 4%PFA to cross link the antibody to the samples; and (2) we stained the sample with secondary antibody after proteinase digestion, with the intention to protect the fluorescent dyes.
Briefly, fixed cells were incubated in primary antibodies for 2 h at room temperature or at 4°C, overnight and then were fixed in 4% PFA for 20 min. After fixation, cells were incubated in the 0.1 mg/ml AcX (Acryloyl-X SE, Invitrogen, cat. no. A20770) solution for 2 to 3 hr at room temperature. Then cells were polymerized in the gelling solution by mixing Stock X (8.6% Sodium acrylate,

2.5% Acrylamide, 0.15% N,N'-Methylenebisacrylamide, 11.7% Sodium chloride, 1x PBS), water, 10% TEMED stock solution, and 10% APS stock solution in a 47:1:1:1 ratio. The gel was then digested with proteinase K (NEB, cat. no. P8107S) at a final concentration of 8 U/ml in digestion buffer (50 mM Tris, pH 8.0, 1 mM EDTA, 0.5% Triton X-100, and 0.8 M NaCl) for 12 h at room temperature. After digestion, proteinase K was removed by four washes with excessive PBS (10 min each time) and the gel was incubated in the secondary antibody for 2 h at room temperature. The post-expansion labeled hydrogel was then washed and expanded by four washes with excessive water (at least 30 min each time) and mounted with superglue. Imaging was performed using an AiryScan LSM880 confocal microscope (Zeiss) with a 63x lens.

During imaging, the elastic nature of the hydrogel makes it difficult to complete a z-stack optical scanning. The short working distance of the lens presses the hydrogel, dislocates the samples' position and causes image blurring. To avoid the potential artifacts of imaging blur, we captured one single optical plane focusing only on the ciliary pocket.

Quantification of cilium length and protein intensity in the cilium

Cilium length was measured in Leica LAS X software. A line was drawn along the fluorescent signal corresponding to the ciliary marker, and the length of this line was defined as the length of the primary cilium. To measure the intensity of protein signal within the cilium, we quantified the average ciliary protein intensity using the CiliaQ plug-in in ImageJ (Hansen et al., 2021). Briefly, we first segmented the channel of cilia labeling into cilia voxels and background voxels with CiliaQ Preparator (V.0.1.1). Manual corrections are made if necessary on the segmentation using CiliaQ Editor (V.0.0.3). The intensity of ciliary proteins in the cilium voxel was then read out from the individual channels of the corresponding proteins in CiliaQ (V.0.1.4).

Quantification of Ptch1 incorporation in Numb-containing CCVs

The quantification was done in Fiji. All quantified images are single focal planes from the AiryScan confocal microscope on cells after expansion microscopy. The region of interest (ROI) was defined as a circle with the cilium base as the center and the cilium length as the radius. Within the ROI, The total number of Numb-containing CCVs are counted, as well as the number of CCVs that incorporate Ptch1.

SDS-PAGE and Western blotting

Standard techniques were used for SDS-PAGE and Western blotting. Cells were first washed with PBS, and then were scraped off from the culture surface in RIPA buffer (1% NP-40, 0.1% SDS, 0.5% sodium deoxycholate, 150 mM NaCl, 25 mM Tris/HCl, pH 7.5, and protease inhibitors). Lysates were cleared by centrifugation (10,000 ×g at 4°C for 15 min), and 25 μg protein was separated on 10% SDS-PAGE gels and transferred onto PVDF membranes. After blocking in 5% BSA, membranes were washed and incubated with primary antibodies and secondary antibodies. Finally, proteins were detected with chemiluminescence substrates (Thermo Fisher Scientific; 34076). Quantitation of bands was performed using ImageJ.

Animals

All animal work was performed in accordance with the Canadian Council on Animal Care Guidelines and approved by the IRCM Animal Care Committee. Mice were maintained in the IRCM specific pathogen-free animal facility. All mice lines have been previously described: *Math1-Cre* (Matei et al., 2005), *numb* conditional allele and *numbl* conditional allele (Wilson et al., 2007) (obtained from The Jackson Laboratory), and *numbl* null allele (Bélanger et al., 2017). Mice of both sexes (not determined) were randomly used for experiments.

For experiments with conditional deletion of *Numb* and *Numbl*, control mice were *Math1-Cre*$^{-}$*;Nb*$^{f/f}$*;NbL*$^{f/f}$*, Math1-Cre*$^{-}$*;Nb*$^{f/f}$*;NbL*$^{f/-}$*, or Math1-Cre*$^{-}$*;Nb*$^{f/-}$*;NbL*$^{f/-}$*. Numb;Numbl* cDKO mice were *Math1-Cre*$^{+}$*;Nb*$^{f/f}$*;Nbl*$^{f/f}$*, Math1-Cre*$^{+}$*;Nb*$^{f/f}$*;Nbl*$^{f/-}$ *or Math1-Cre*$^{+}$*;Nb*$^{f/-}$*;Nbl*$^{f/-}$.

Histology

Brains were dissected and fixed by immersion overnight in 4% paraformaldehyde (PFA) diluted in PBS. The tissues were then cryoprotected in 30% sucrose, embedded in a sucrose:OCT (1:1) mix and frozen. Histology and immunochemistry were performed on sections as described previously (Charron et al., 2003; Izzi et al., 2011). Rabbit anti-Numb antibody (Abcam 14140) was used at 1:250.

Isolation of GCPs and in vitro proliferation assays

GCPs were isolated from P6 mice cerebella as described previously (Izzi et al., 2011; Wechsler-Reya and Scott, 1999). Briefly, isolated cerebella were cut into small pieces and treated with trypsin and DNase I. After trituration, single cell suspensions were centrifuged through a 30% to 65% percoll step gradient. Cells were harvested at the 30% interphase and then resuspended in Neurobasal supplemented with B27, 0.5 mM L-glutamine and penicillin/streptomycin and plated on plates precoated with 100 µg/ml poly-D-Lysine.

For the ^{3}H-thymidine incorporation assay, GCPs were plated at 3 X 10^{5} cells per well in 96 well plates in triplicate and treated with ShhN for 48 h. GCPs were pulsed with 1 µCi/ml ^{3}H-thymidine 12 hours after seeding the cells. The amount of ^{3}H-thymidine incorporation was measured using the Filtermate harvester (PerkinElmer).

Cell cycle assay

The cell cycle time of cells in control and *Numb;Numbl* cDKO mice was measured as described previously (Das et al., 2009). Cells were exposed to BrdU (5-bromo-2'-deoxy-uridine) for 2 h, followed by EdU (5-ethynyl-2'-deoxy-uridine) for 30 min. The BrdU+ EdU- cells represent cells which were in S phase during the initial 2 h but exited S phase for the last 30 min. PCNA was used at to identify cells in all phases of the cell cycle

Statistical analyses

Statistical analyses were performed with GraphPad Prism 8. For volcano plot graphs, Student's t-test were used and statistical analyses were performed in Prism 8. Hierarchical cluster analyses were performed according to Ward's minimum variance method.

REFERENCES

Abdi, K., Neves, G., Pyun, J., Kiziltug, E., Ahrens, A., and Kuo, C.T. (2019). EGFR Signaling Termination via Numb Trafficking in Ependymal Progenitors Controls Postnatal Neurogenic Niche Differentiation. Cell Rep. *28*, 2012-2022.e4.

Arveseth, C.D., Happ, J.T., Hedeen, D.S., Zhu, J.F., Capener, J.L., Shaw, D.K., Deshpande, I., Liang, J., Xu, J., Stubben, S.L., et al. (2021). Smoothened transduces hedgehog signals via activity-dependent sequestration of PKA catalytic subunits.

Bélanger, M.-C., Robert, B., and Cayouette, M. (2017). Msx1-Positive Progenitors in the Retinal Ciliary Margin Give Rise to Both Neural and Non-neural Progenies in Mammals. Dev. Cell *40*, 137–150.

Branon, T.C., Bosch, J.A., Sanchez, A.D., Udeshi, N.D., Svinkina, T., Carr, S.A., Feldman, J.L., Perrimon, N., and Ting, A.Y. (2018). Efficient proximity labeling in living cells and organisms with TurboID. Nat. Biotechnol. *36*, 880–887.

Charron, F., Stein, E., Jeong, J., McMahon, A.P., and Tessier-Lavigne, M. (2003). The Morphogen Sonic Hedgehog Is an Axonal Chemoattractant that Collaborates with Netrin-1 in Midline Axon Guidance. Cell *113*, 11–23.

Corbit, K.C., Aanstad, P., Singla, V., Norman, A.R., Stainier, D.Y.R., and Reiter, J.F. (2005). Vertebrate Smoothened functions at the primary cilium. Nature *437*, 1018–1021.

Dahmane, N., and Ruiz-i-Altaba, A. (1999). Sonic hedgehog regulates the growth and patterning of the cerebellum. Development *126*, 3089–3100.

Das, G., Choi, Y., Sicinski, P., and Levine, E.M. (2009). Cyclin D1 fine-tunes the neurogenic output of embryonic retinal progenitor cells. Neural Dev. *4*, 15.

Deshpande, I., Liang, J., Hedeen, D., Roberts, K.J., Zhang, Y., Ha, B., Latorraca, N.R., Faust, B., Dror, R.O., Beachy, P.A., et al. (2019). Smoothened stimulation by membrane sterols drives Hedgehog pathway activity. Nature *571*, 284–288.

Dorn, K. V., Hughes, C.E., and Rohatgi, R. (2012). A Smoothened-Evc2 Complex Transduces the Hedgehog Signal at Primary Cilia. Dev. Cell *23*, 823–835.

Eggenschwiler, J.T., and Anderson, K. V. (2007). Cilia and Developmental Signaling. Annu. Rev. Cell Dev. Biol. *23*, 345–373.

Elias, J.E., and Gygi, S.P. (2007). Target-decoy search strategy for increased confidence in large-scale protein identifications by mass spectrometry. Nat. Methods *4*, 207–214.

Ferent, J., Giguère, F., Jolicoeur, C., Morin, S., Michaud, J.-F., Makihara, S., Yam, P.T., Cayouette, M., and Charron, F. (2019). Boc Acts via Numb as a Shh-Dependent Endocytic Platform for Ptch1 Internalization and Shh-Mediated Axon Guidance. Neuron *102*, 1157-1171.e5.

Ghossoub, R., Molla-Herman, A., Bastin, P., and Benmerah, A. (2011). The ciliary pocket: a once-forgotten membrane domain at the base of cilia. Biol. Cell *103*, 131–144.

Goetz, S.C., and Anderson, K. V. (2010). The primary cilium: a signalling centre during vertebrate development. Nat. Rev. Genet. *11*, 331–344.

Hansen, J.N., Rassmann, S., Stüven, B., Jurisch-Yaksi, N., and Wachten, D. (2021). CiliaQ: a simple, open-source software for automated quantification of ciliary morphology and fluorescence in 2D, 3D, and 4D images. Eur. Phys. J. E *44*, 18.

Huang, P., Nedelcu, D., Watanabe, M., Jao, C., Kim, Y., Liu, J., and Salic, A. (2016). Cellular Cholesterol Directly Activates Smoothened in Hedgehog Signaling. Cell *166*, 1176-1187.e14.

Huangfu, D., Liu, A., Rakeman, A.S., Murcia, N.S., Niswander, L., and Anderson, K. V. (2003). Hedgehog signalling in the mouse requires intraflagellar transport proteins. Nature *426*, 83–87.

Hung, V., Udeshi, N.D., Lam, S.S., Loh, K.H., Cox, K.J., Pedram, K., Carr, S.A., and Ting, A.Y. (2016). Spatially resolved proteomic mapping in living cells with the engineered peroxidase APEX2. Nat. Protoc. *11*, 456–475.

Izzi, L., Lévesque, M., Morin, S., Laniel, D., Wilkes, B.C., Mille, F., Krauss, R.S., McMahon, A.P., Allen, B.L., and Charron, F. (2011). Boc and Gas1 Each Form Distinct Shh Receptor Complexes with Ptch1 and Are Required for Shh-Mediated Cell Proliferation. Dev. Cell *20*, 788–801.

Kechad, A., Jolicoeur, C., Tufford, A., Mattar, P., Chow, R.W.Y., Harris, W.A., and Cayouette, M. (2012). Numb is Required for the Production of Terminal Asymmetric Cell Divisions in the Developing Mouse Retina. J. Neurosci. *32*, 17197–17210.

Kim, J., Kato, M., and Beachy, P.A. (2009). Gli2 trafficking links Hedgehog-dependent activation of Smoothened in the primary cilium to transcriptional activation in the nucleus. Proc. Natl. Acad. Sci. *106*, 21666–21671.

Kim, J., C. Hsia, E.Y., Brigui, A., Plessis, A., Beachy, P.A., and Zheng, X. (2015). The role of ciliary trafficking in Hedgehog receptor signaling. Sci. Signal. *8*, 1–9.

Klein, A.-L., Zilian, O., Suter, U., and Taylor, V. (2004). Murine numb regulates granule cell maturation in the cerebellum. Dev. Biol. *266*, 161–177.

Kohli, P., Höhne, M., Jüngst, C., Bertsch, S., Ebert, L.K., Schauss, A.C., Benzing, T., Rinschen, M.M., and Schermer, B. (2017). The ciliary membrane-associated proteome reveals actin-binding proteins as key components of cilia. EMBO Rep. *18*, 1521–1535.

Kong, J.H., Siebold, C., and Rohatgi, R. (2019). Biochemical mechanisms of vertebrate hedgehog signaling. Development *146*, dev166892.

Larkins, C.E., Aviles, G.D.G., East, M.P., Kahn, R.A., and Caspary, T. (2011). Arl13b regulates ciliogenesis and the dynamic localization of Shh signaling proteins. Mol. Biol. Cell *22*, 4694–4703.

Li, H.S., Wang, D., Shen, Q., Schonemann, M.D., Gorski, J.A., Jones, K.R., Temple, S., Jan, L.Y., and Jan, Y.N. (2003). Inactivation of Numb and Numblike in embryonic dorsal forebrain impairs neurogenesis and disrupts cortical morphogenesis. Neuron *40*, 1105–1118.

Li, J., Van Vranken, J.G., Pontano Vaites, L., Schweppe, D.K., Huttlin, E.L., Etienne, C., Nandhikonda, P., Viner, R., Robitaille, A.M., Thompson, A.H., et al. (2020). TMTpro reagents: a set of isobaric labeling mass tags enables simultaneous proteome-wide measurements across 16 samples. Nat. Methods *17*, 399–404.

Lu, H., Toh, M.T., Narasimhan, V., Thamilselvam, S.K., Choksi, S.P., and Roy, S. (2015a). A

function for the Joubert syndrome protein Arl13b in ciliary membrane extension and ciliary length regulation. Dev. Biol. *397*, 225–236.

Lu, Q., Insinna, C., Ott, C., Stauffer, J., Pintado, P.A., Rahajeng, J., Baxa, U., Walia, V., Cuenca, A., Hwang, Y.S., et al. (2015b). Early steps in primary cilium assembly require EHD1/EHD3-dependent ciliary vesicle formation. Nat. Cell Biol. *17*, 228–240.

Marcotullio, L. Di, Ferretti, E., Greco, A., De Smaele, E., Po, A., Sico, M.A., Alimandi, M., Giannini, G., Maroder, M., Screpanti, I., et al. (2006). Numb is a suppressor of Hedgehog signalling and targets Gli1 for Itch-dependent ubiquitination. Nat. Cell Biol. *8*, 1415–1423.

Matei, V., Pauley, S., Kaing, S., Rowitch, D., Beisel, K.W., Morris, K., Feng, F., Jones, K., Lee, J., and Fritzsch, B. (2005). Smaller inner ear sensory epithelia in Neurog1 null mice are related to earlier hair cell cycle exit. Dev. Dyn. *234*, 633–650.

May, E.A., Kalocsay, M., Auriac, I.G.D., Schuster, P.S., Gygi, S.P., Nachury, M. V, and Mick, D.U. (2021). Time-resolved proteomics profiling of the ciliary Hedgehog response. J. Cell Biol. *220*, e202007207.

Mick, D.U., Rodrigues, R.B., Leib, R.D., Adams, C.M., Chien, A.S., Gygi, S.P., and Nachury, M. V. (2015). Proteomics of Primary Cilia by Proximity Labeling. Dev. Cell *35*, 497–512.

Milenkovic, L., Scott, M.P., and Rohatgi, R. (2009). Lateral transport of Smoothened from the plasma membrane to the membrane of the cilium. J. Cell Biol. *187*, 365–374.

Molla-Herman, A., Ghossoub, R., Blisnick, T., Meunier, A., Serres, C., Silbermann, F., Emmerson, C., Romeo, K., Bourdoncle, P., Schmitt, A., et al. (2010). The ciliary pocket: An endocytic membrane domain at the base of primary and motile cilia. J. Cell Sci. *123*, 1785–1795.

Nishimura, T., and Kaibuchi, K. (2007). Numb Controls Integrin Endocytosis for Directional Cell Migration with aPKC and PAR-3. Dev. Cell *13*, 15–28.

Nozaki, S., Katoh, Y., Terada, M., Michisaka, S., Funabashi, T., Takahashi, S., Kontani, K., and Nakayama, K. (2016). Regulation of ciliary retrograde protein trafficking by Joubert syndrome proteins ARL13B and INPP5E. J. Cell Sci. *3*, 563–576.

Petersen, P.H., Zou, K., Hwang, J.K., Jan, Y.N., and Zhong, W. (2002). Progenitor cell maintenance requires numb and numblike during mouse neurogenesis. Nature *419*, 929–934.

Raleigh, D.R., Sever, N., Choksi, P.K., Sigg, M.A., Hines, K.M., Thompson, B.M., Elnatan, D., Jaishankar, P., Bisignano, P., Garcia-Gonzalo, F.R., et al. (2018). Cilia-Associated Oxysterols Activate Smoothened. Mol. Cell *72*, 316-327.e5.

Reiter, J.F., Blacque, O.E., and Leroux, M.R. (2012). The base of the cilium: roles for transition fibres and the transition zone in ciliary formation, maintenance and compartmentalization. EMBO Rep. *13*, 608–618.

Roegiers, F., and Jan, Y.N. (2004). Asymmetric cell division. Curr. Opin. Cell Biol. *16*, 195–205.

Rohatgi, R., and Snell, W.J. (2010). The Ciliary Membrane. Curr. Opin. Cell Biol. *22*, 541–546.

Rohatgi, R., Milenkovic, L., and Scott, M.P. (2007). Patched1 regulates hedgehog signaling at the primary cilium. Science (80-.). *317*, 372–376.

Roux, K.J., Kim, D.I., Raida, M., and Burke, B. (2012). A promiscuous biotin ligase fusion protein identifies proximal and interacting proteins in mammalian cells. J. Cell Biol. *196*, 801–810.

Roy, K., Jerman, S., Jozsef, L., McNamara, T., Onyekaba, G., Sun, Z., and Marin, E.P. (2017). Palmitoylation of the ciliary GTPase ARL13b is necessary for its stability and its role in cilia formation. J. Biol. Chem. *292*, 17703–17717.

Rudolf, A.F., Kinnebrew, M., Kowatsch, C., Ansell, T.B., El Omari, K., Bishop, B., Pardon, E., Schwab, R.A., Malinauskas, T., Qian, M., et al. (2019). The morphogen Sonic hedgehog inhibits its receptor Patched by a pincer grasp mechanism. Nat. Chem. Biol. *15*, 975–982.

Shiba, D., Yamaoka, Y., Hagiwara, H., Takamatsu, T., Hamada, H., and Yokoyama, T. (2009). Localization of Inv in a distinctive intraciliary compartment requires the C-terminal ninein-homolog-containing region. J. Cell Sci. *122*, 44–54.

Stump, G., Durrer, A., Klein, A.-L., Lütolf, S., Suter, U., and Taylor, V. (2002). Notch1 and its ligands Delta-like and Jagged are expressed and active in distinct cell populations in the postnatal mouse brain. Mech. Dev. *114*, 153–159.

Tamayo-Orrego, L., Gallo, D., Racicot, F., Bemmo, A., Mohan, S., Ho, B., Salameh, S., Hoang, T., Jackson, A.P., Brown, G.W., et al. (2020). Sonic hedgehog accelerates DNA replication to cause replication stress promoting cancer initiation in medulloblastoma. Nat. Cancer *1*, 840–854.

Tillberg, P.W., Chen, F., Piatkevich, K.D., Zhao, Y., Yu, C.-C., English, B.P., Gao, L., Martorell, A., Suk, H.-J., Yoshida, F., et al. (2016). Protein-retention expansion microscopy of cells and tissues labeled using standard fluorescent proteins and antibodies. Nat. Biotechnol. *34*, 987–992.

Wallace, V.A. (1999). Purkinje-cell-derived Sonic hedgehog regulates granule neuron precursor cell proliferation in the developing mouse cerebellum. Curr. Biol. *9*, 445–448.

Wassie, A.T., Zhao, Y., and Boyden, E.S. (2019). Expansion microscopy: principles and uses in biological research. Nat. Methods *16*, 33–41.

Wechsler-Reya, R.J., and Scott, M.P. (1999). Control of Neuronal Precursor Proliferation in the Cerebellum by Sonic Hedgehog. Neuron *22*, 103–114.

Wilson, A., Ardiet, D.-L., Saner, C., Vilain, N., Beermann, F., Aguet, M., MacDonald, H.R., and Zilian, O. (2007). Normal Hemopoiesis and Lymphopoiesis in the Combined Absence of Numb and Numblike. J. Immunol. *178*, 6746–6751.

Xie, J., Murone, M., Luoh, S.-M., Ryan, A., Gu, Q., Zhang, C., Bonifas, J.M., Lam, C.-W., Hynes, M., Goddard, A., et al. (1998). Activating Smoothened mutations in sporadic basal-cell carcinoma. Nature *391*, 90–92.

Yap, C.C., and Winckler, B. (2015). Adapting for endocytosis: roles for endocytic sorting adaptors in directing neural development. Front. Cell. Neurosci. *9*, 1–17.

Yue, S., Tang, L.-Y., Tang, Y., Tang, Y., Shen, Q.-H., Ding, J., Chen, Y., Zhang, Z., Yu, T.-T., Zhang, Y.E., et al. (2014). Requirement of Smurf-mediated endocytosis of Patched1 in sonic hedgehog signal reception. Elife *3*, 1–24.

Zhang, Y., Bulkley, D.P., Xin, Y., Roberts, K.J., Asarnow, D.E., Sharma, A., Myers, B.R., Cho,

W., Cheng, Y., and Beachy, P.A. (2018). Structural Basis for Cholesterol Transport-like Activity of the Hedgehog Receptor Patched. Cell *175*, 1352-1364.e14.

Zhong, W., Jiang, M.-M., Schonemann, M.D., Meneses, J.J., Pedersen, R.A., Jan, L.Y., and Jan, Y.N. (2000). Mouse numb is an essential gene involved in cortical neurogenesis. Proc. Natl. Acad. Sci. *97*, 6844–6849.

Zhou, P., Alfaro, J., Chang, E.H., Zhao, X., Porcionatto, M., and Segal, R.A. (2011). Numb links extracellular cues to intracellular polarity machinery to promote chemotaxis. Dev. Cell *20*, 610–622.

Zuzow, N., Ghosh, A., Leonard, M., Liao, J., Yang, B., and Bennett, E.J. (2018). Mapping the mammalian ribosome quality control complex interactome using proximity labeling approaches. Mol. Biol. Cell *29*, 1258–1269.

Figures

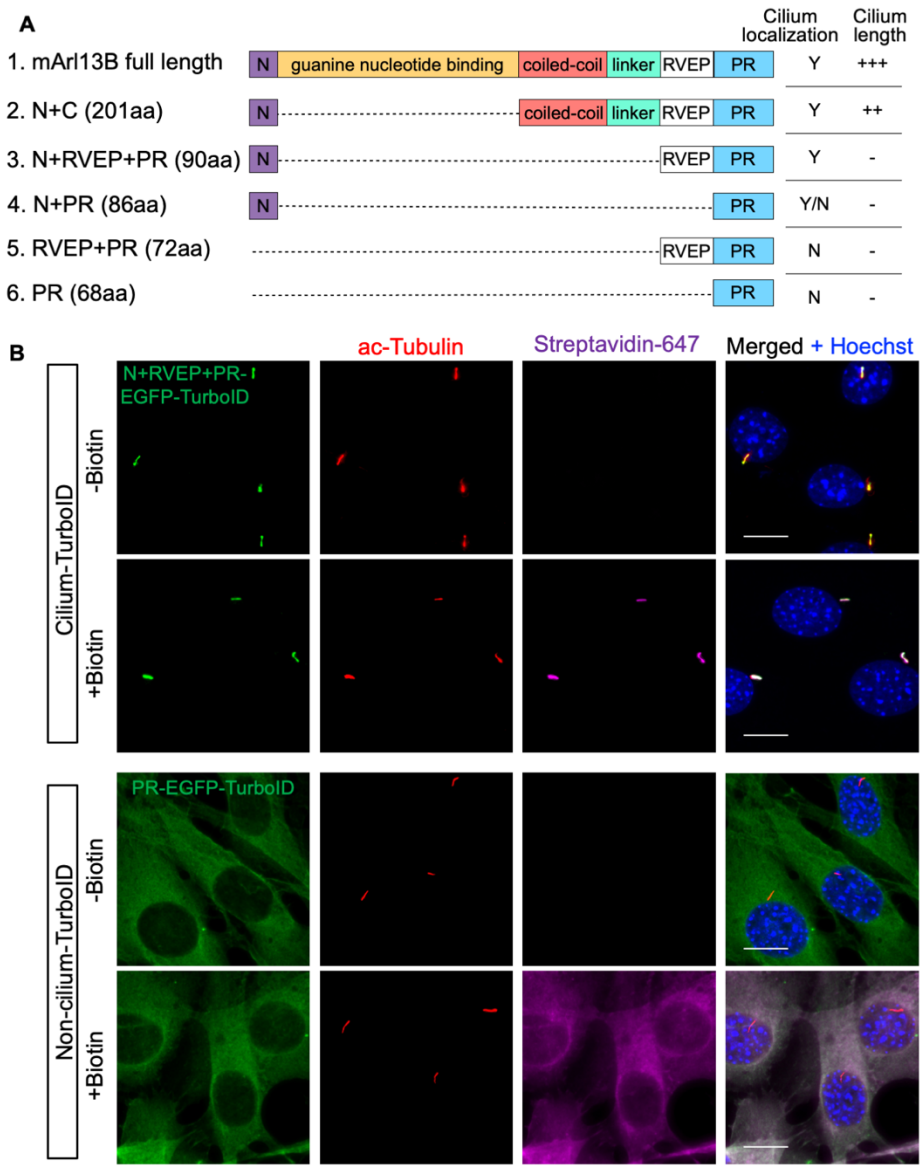

Figure 1. Cilium-TurboID selectively biotinylates ciliary proteins.
(**A**) Schematics of the truncated Arl13b constructs used. Y and N indicate whether the corresponding construct localizes to the cilium or not, respectively. Y/N: this construct localizes to both the cilium and the cytosol. "+": the degree of cilium elongation in NIH3T3 cells transiently transfected with the corresponding constructs. "-": cilium length is not impacted.
(**B**) Immunofluorescence of stable NIH3T3 cell lines expressing cilium-TurboID (N+RVEP-PR-EGFP-TurboID) or non-cilium-TurboID (PR-EGFP-TurboID) before and after biotin labeling. Cells were serum-starved for 24 h, incubated with 50 μM biotin for 10 min at 37°C, and fixed for immunostaining. The cilium is labeled by immunostaining for acetylated-tubulin (red, ac-tubulin), and the biotinylated proteins were detected via streptavidin-Alexa Fluor 647 (magenta). Cilium-TurboID and non-cilium TurboID were detected by immunostaining for EGFP (green). Scale bars, 10 μm in all panels.

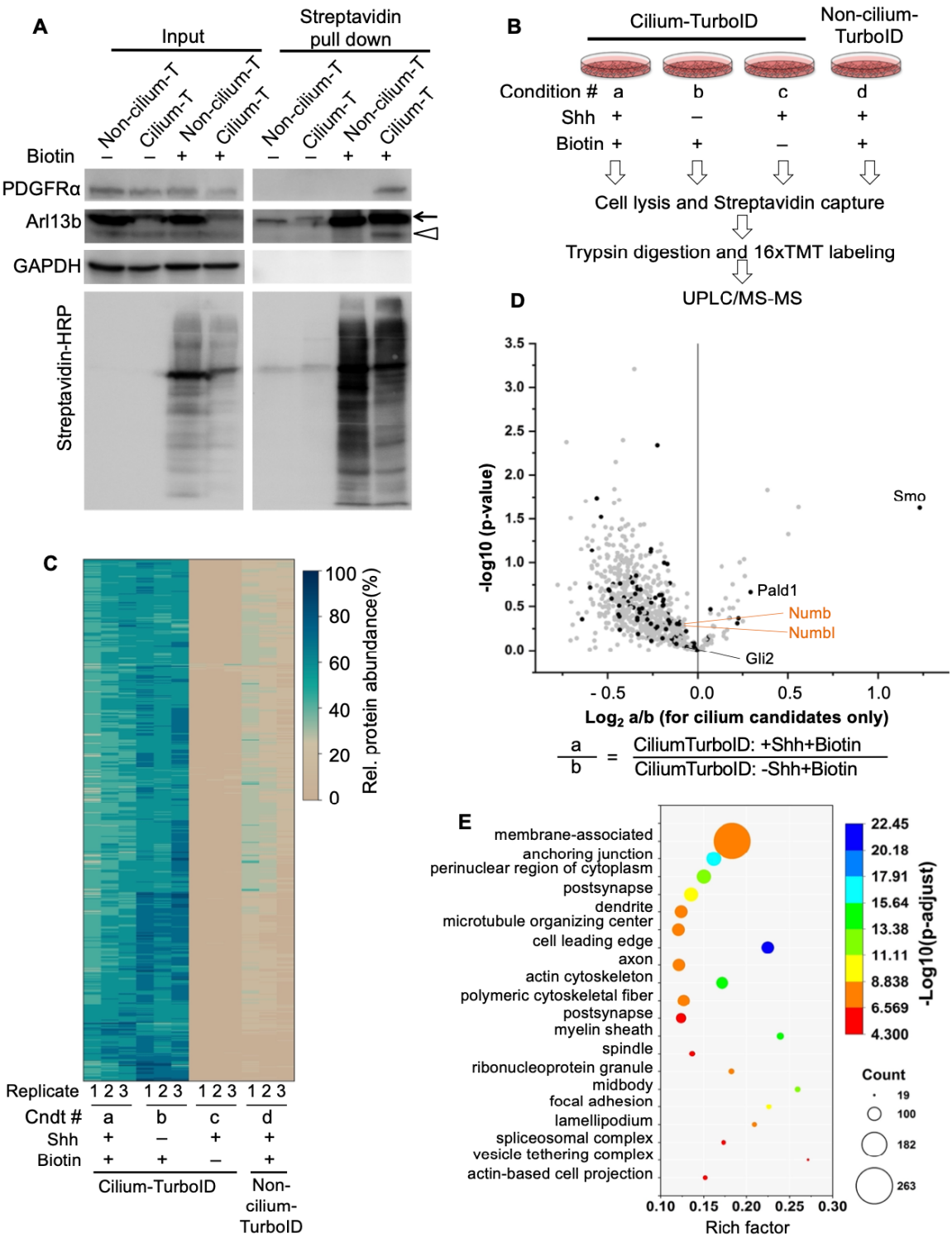

Figure 2. Quantitative proteomics with cilium-TurboID identified novel ciliary proteins. (**A**) Biotinylated proteins from cell lysates of cilium-TurboID and non-cilium-TurboID cells were isolated by streptavidin beads and analyzed by Western blotting. The overall biotinylated proteins were detected by streptavidin-HRP. PDGFRα is a receptor known to localize to the cilium. In Arl13b blot, the arrow points to the transgene, and the triangle points to endogenous Arl13b.

(**B**) Design and workflow of the cilium proteomics experiment. Samples were prepared in triplicate. After TMT labeling, all samples were pooled together before being fractionated by UPLC and analyzed by mass spectrometry.
(**C**) Heatmap of the ciliary abundance of the 800 ciliary candidates. Clustering of the relative abundances of each identified protein (rows) in individual samples (columns) was performed based on Ward's minimum variance method. The relative abundance was calculated within one set of samples that contains all four conditions. For example, a1, b1, c1, d1 belong to one set, and the relative abundance is calculated as a1/(a1+b1+c1+d1) etc. Right, the color scheme of relative abundances (percentage).
(**D**) Volcano plot of statistical significance versus the average ratio of protein enrichment for all ciliary candidates. The ratio was calculated as TMT signal intensity of Shh-treated samples (a) compared to none-Shh samples (b) in the presence of biotin labeling. The analytical procedure for identifying ciliary candidates from the mass spectrometry results is described in Fig. S3A-D. The previously reported ciliary proteins are highlighted as black dots.
(**E**) GO enrichment analysis of cellular components was plotted according to the rich factor in Metascape. The top 20 enriched cellular components are represented in the scatter plot.

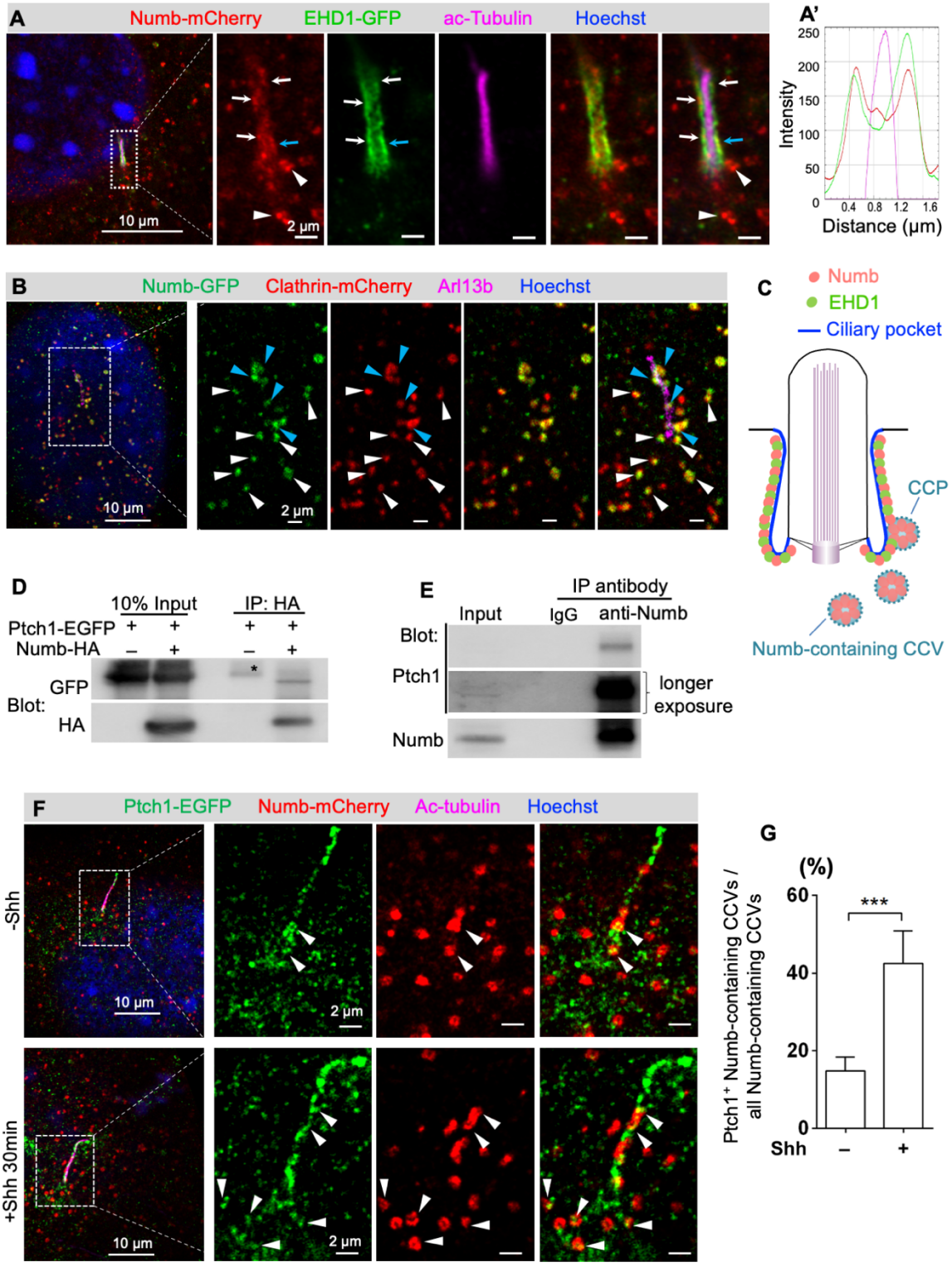

Figure 3. Numb localizes to the ciliary pocket and incorporates Ptch1 into clathrin coated vesicles.

(**A**) Numb localizes to the ciliary pocket in NIH3T3 cells. Cells were co-transfected with Numb-mCherry and EHD1-GFP, physically expanded via expansion microscopy, and imaged with an

Airyscan confocal microscope. The image shown is from a single focal plane, and only the bottom portion of the cilium axoneme is in the focal plane. The cilium axoneme is labeled with acetylated (ac)-tubulin immunostaining. Arrows point to the ciliary pocket where Numb and EHD1 colocalize; white triangles point to the Numb-containing puncta near the base of the cilium.
(A') The linescan was performed at the position marked by the cyan arrow to show colocalization of Numb with EHD1 in the ciliary pocket. Red: Numb-mCherry, green: EHD1-GFP, magenta: ac-tubulin.
(**B**) Numb localizes to clathrin coated vesicles (CCVs). Cells were co-transfected with Numb-GFP and clathrin-mCherry, processed via expansion microscopy, and imaged with an Airyscan confocal microscope. The image shown is single focal plane focusing on the CCVs near the base of the cilium. The cilium membrane is labeled by Arl13b immunostaining. White triangles point to the Numb-containing CCVs. Cyan triangles point to Numb-containing CCVs associated with the ciliary pocket, which are potentially clathrin coated pits (CCPs).
(C) The diagram illustrating Numb localization to the ciliary pocket, to CCPs associated with the ciliary pocket, and to CCVs near the base of the cilium.
(**D**) Ptch1-EGFP and Numb-HA were expressed in 293T cells. Numb-HA was immunoprecipitated with an anti-HA antibody, and Ptch1-EGFP was co-immunoprecipitated with Numb-HA. * indicates a non-specific band.
(**E**) In ciliated NIH3T3 cells, endogenous Ptch1 was co-immunoprecipitated with endogenous Numb protein by Numb antibody.
(**F**) Ptch1 is incorporated into Numb-containing CCVs at the ciliary pocket. Cells were co-transfected with Ptch1-EGFP and Numb-mCherry, treated with Shh or vehicle for 30 min before fixation. Cells went through expansion microscopy and were imaged in an Airyscan confocal microscope. Only a single focal plane is shown. White triangles point to Numb-containing CCVs that incorporate Ptch1. Shh stimulation increases the percentage of Numb-containing CCVs that incorporate Ptch1.
(**G**) Quantification of Ptch1 localization in Numb-containing CCVs. n = 5 cells per condition. Unpaired two-tailed t-test. ***, $p < 0.001$. All error bars depict SD.

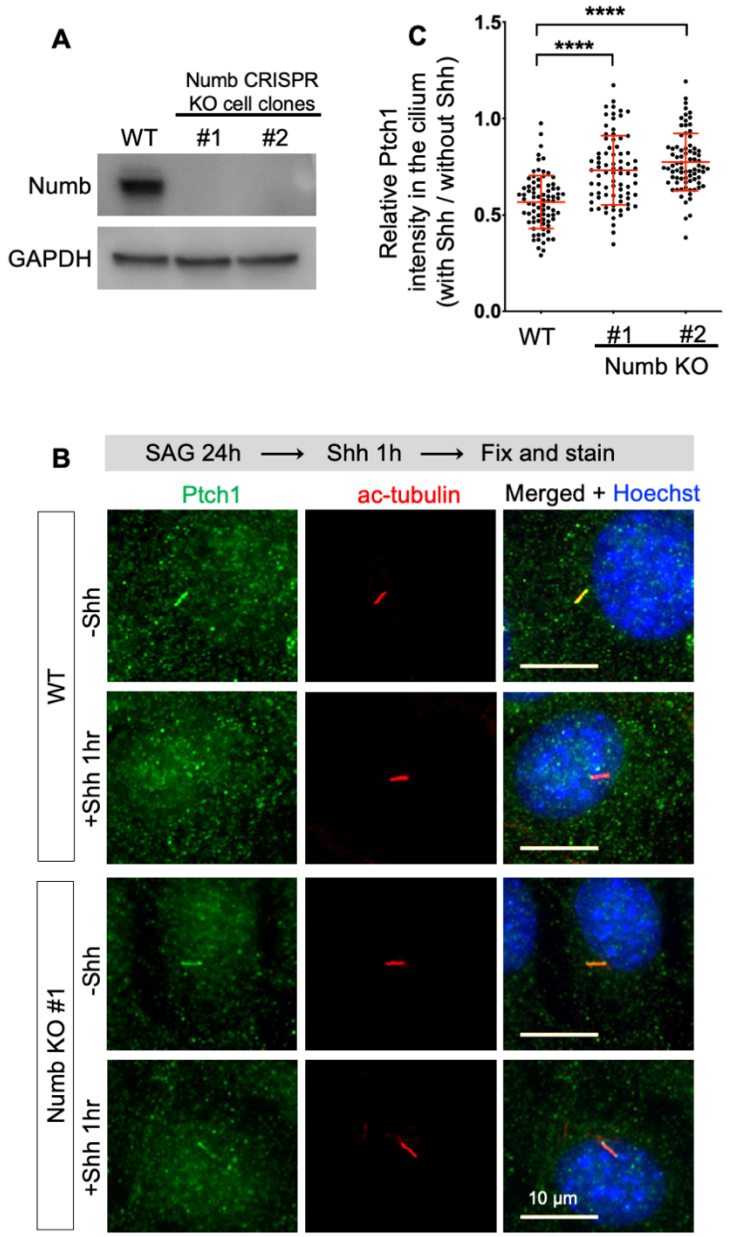

Figure 4. Numb is required for Shh-induced Ptch1 exit from the cilium.

(A) Western blot showing that Numb protein was non-detectable in Numb CRISPR/cas9 knockout cell clones.

(B) Immunofluorescence staining of endogenous Ptch1 in the cilia of WT or Numb KO cells with and without Shh stimulation. Cells were pretreated with SAG for 24hr to induce Ptch1 expression and stimulated with Shh for 1 h before being fixed for immunostaining. Cilia were labeled by immunostaining for ac-tubulin.

(C) Quantification of endogenous Ptch1 intensity in the cilium. Data are presented as the ratio of ciliary Ptch1 intensity in individual cells stimulated with Shh over the mean ciliary Ptch1 intensity in unstimulated cells of the corresponding cell strains. Data are shown as mean ± SD. n = 50 cilia per condition. One-way ANOVA with multiple comparisons (Tukey test). ****, $p < 0.0001$. Scale bars, 10 µm in all panels.

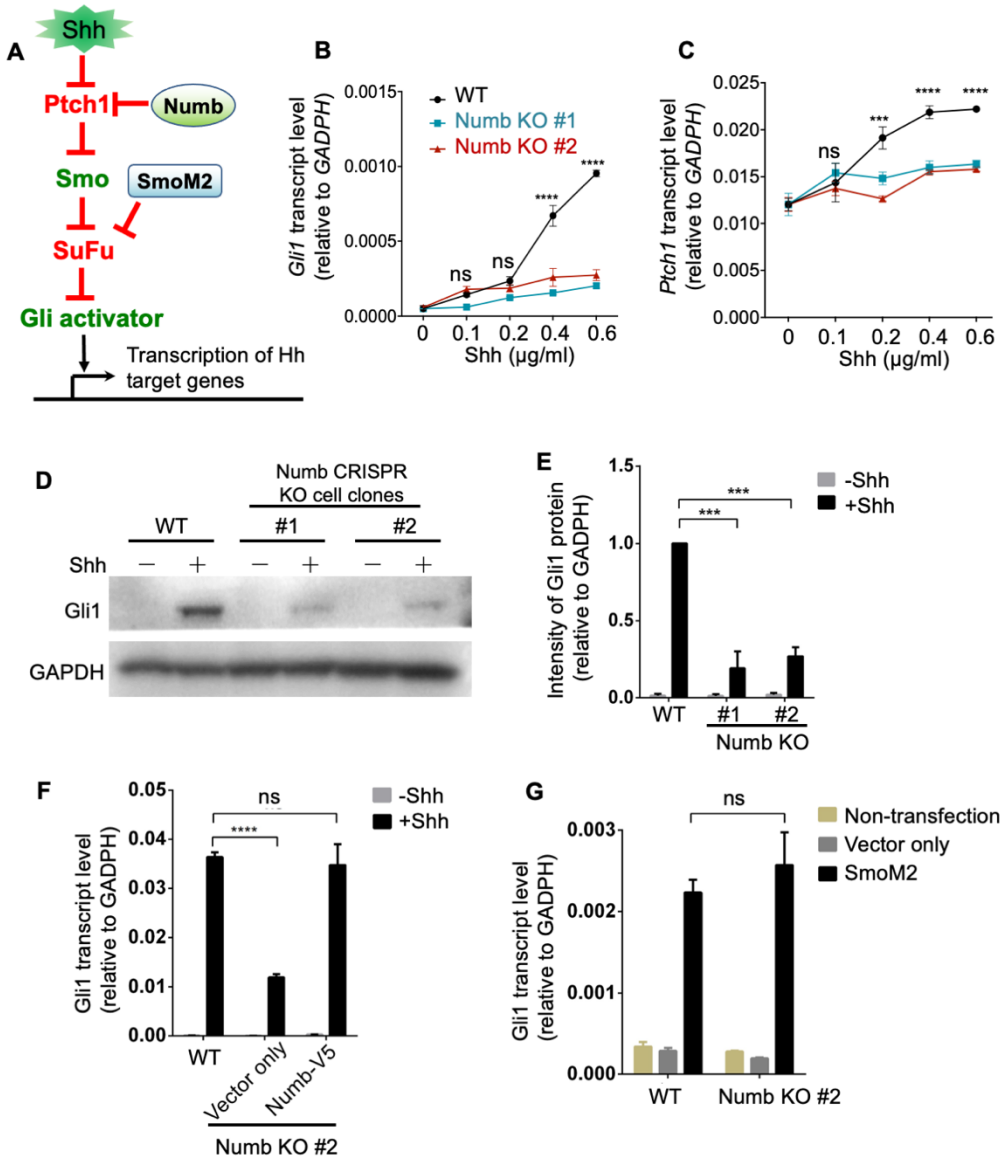

Figure 5. Numb is required for activation of Hh signaling.

(**A**) Diagram of the Hh signaling cascade showing that Numb regulates Hh signaling at the level of Ptch1.

(B-C) qPCR of the transcript levels of the Hh-target genes *Gli1* and *Ptch1*. The target gene transcription was severely reduced at high doses of Shh, but not at low doses.

(**D-E**) Western blot and quantification of Gli1 protein shows that Shh-induced Gli1 protein levels are severely reduced in Numb KO cells.

(**F**) When Numb-V5 are expressed in Numb KO cells, Shh-induced *Gli1* transcription is restored to a level comparable to that in WT cells. *Gli1* transcript levels were determined with qPCR.

(**G**) SmoM2 activates Hh signaling in Numb KO cells. Hh signaling activity is assessed by *Gli1* transcript levels.

(**B, C, E, F, G**): Two-way ANOVA with multiple comparisons (Tukey test). All error bars represent SD, n = 4. ***, $p < 0.001$. ns, not significant.

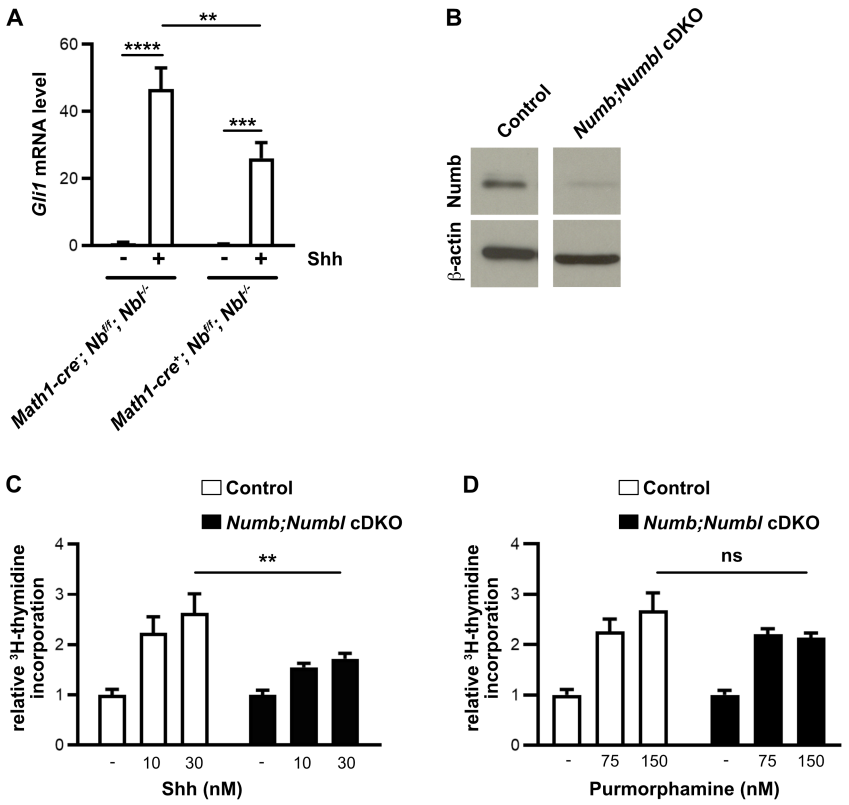

Figure 6. Numb is expressed in GCPs and is required for Hh signaling and Hh-induced proliferation.

(A) GCPs were isolated from P6 mice and cultured in the absence or presence of 1 nM Shh for 20 h. mRNA was isolated from the GCPs and *Gli1* mRNA levels measured by qRT-PCR, relative to *Gusb* gene. The absence of Numb/Numbl reduces the levels of Gli1 induction by Shh (n ≥ 5 animals per genotype).

(B) GCPs were isolated from the cerebella of control and *Numb;Numbl* cDKO mice and the cell lysates analysed by SDS-PAGE followed by Western blotting. Numb expression is almost completely ablated in *Numb;Numbl* cDKO cerebellum.

(C-D) GCPs isolated from the cerebellum of P6 control and *Numb;Numbl* cDKO mice were cultured for 48 h in the presence of **(C)** 0, 10 nM or 30 nM Shh or **(D)** 0, 75 nM and 150 nM purmorphamine. GCP proliferation was measured by the amount of ^{3}H-thymidine incorporation. The levels of ^{3}H-thymidine incorporation were calculated relative to the ^{3}H-thymidine incorporation in untreated GCPs. n ≥ 3 cerebella per group. Numb is required for the maximum proliferative response to Shh, but not to purmorphamine. Two-way ANOVA, ** = $p < 0.01$, *** = $p < 0.001$, **** = $p < 0.0001$, ns = not significant

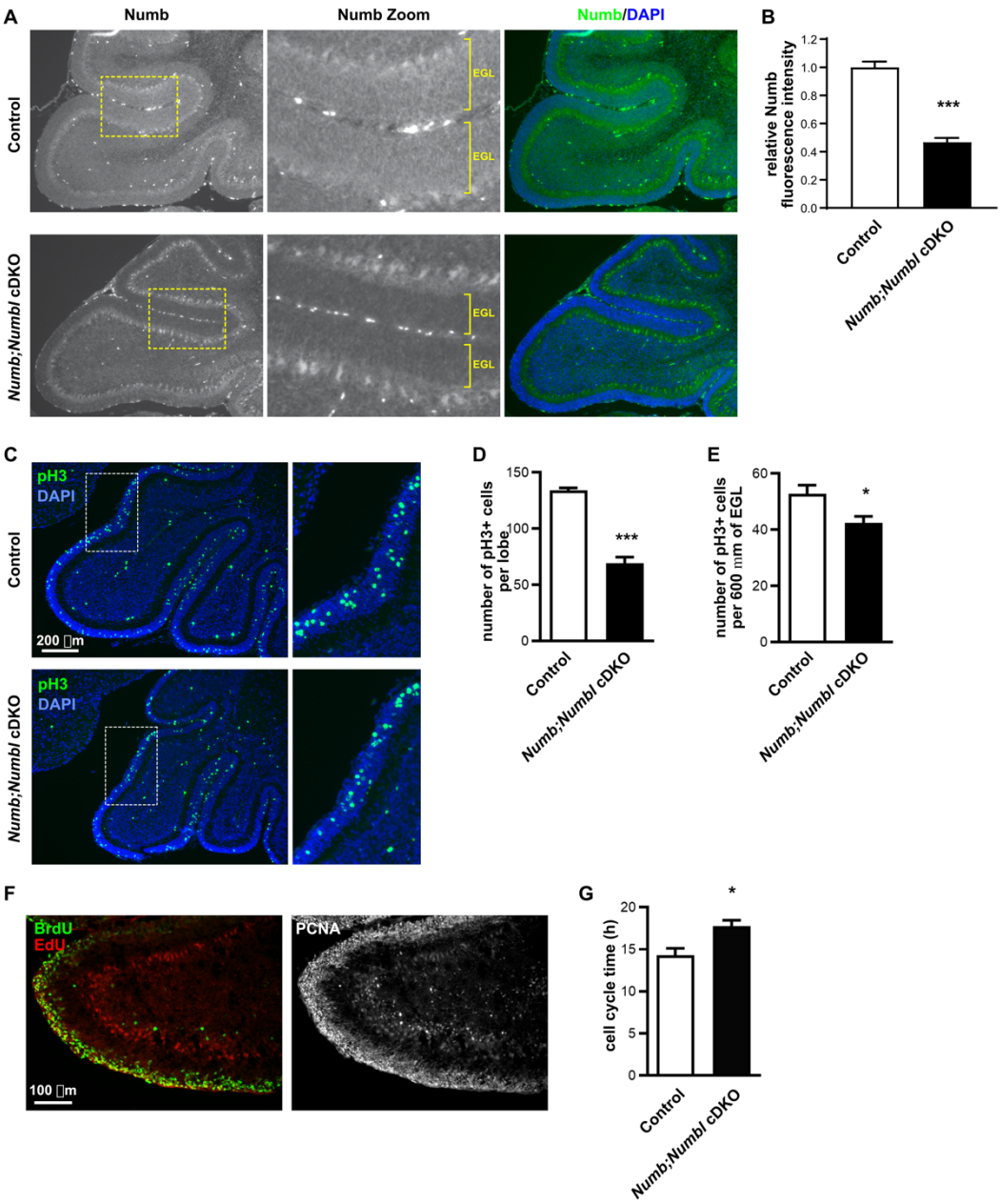

Figure 7. *Numb/Numbl* cDKO mice have reduced cell proliferation in the EGL of the cerebellum.

(A) Sagittal sections of cerebellum from P6 control and *Numb;Numbl* cDKO mice immunostained for Numb. Numb is most strongly expressed in the EGL and the Purkinje cells. The Numb immunostaining fluorescence intensity in the EGL of *Numb;Numbl* cDKO cerebellum is much lower than in the control cerebellum. Boxes indicate the zoomed regions. The EGL, external granule layer, is denoted by brackets.

(B) Quantification of the mean Numb fluorescence intensity (±s.e.m.) in the EGL of control and *Numb;Numbl* cDKO cerebellum. n ≥ 3 cerebella/group. Student's t-test, *** = $p<0.001$.

(C) Sagittal sections of cerebellum from P6 control and *Numb;Numbl* cDKO mice immunostained for the mitotic marker pH3. Boxes indicate the zoomed regions.

(D) Quantification of the number (mean ±s.e.m) of $pH3^+$ cells in the EGL in one lobe of the cerebellum, and **(E)** $pH3^+$ cells/600 µm path along the EGL. n ≥ 3 cerebella per group. Deletion of *Numb* and *Numbl* results in fewer proliferating GCPs in the EGL compared to control.
(F) Immunostaining of sagittal sections of cerebellum pulse labeled with BrdU and EdU which allows the estimation of the GCP cell cycle time.
(G) Quantification of the length of cell cycle (±s.e.m) in GCPs of control and *Numb;Numbl* cDKO cerebellum. The cell cycle length is calculated with this equation: 2h × ($PCNA^+$ cells/$BrdU^+EdU^-$ cells). n = 3 cerebella per group. Student's t-test, *** = $p<0.001$; *= $p<0.05$.

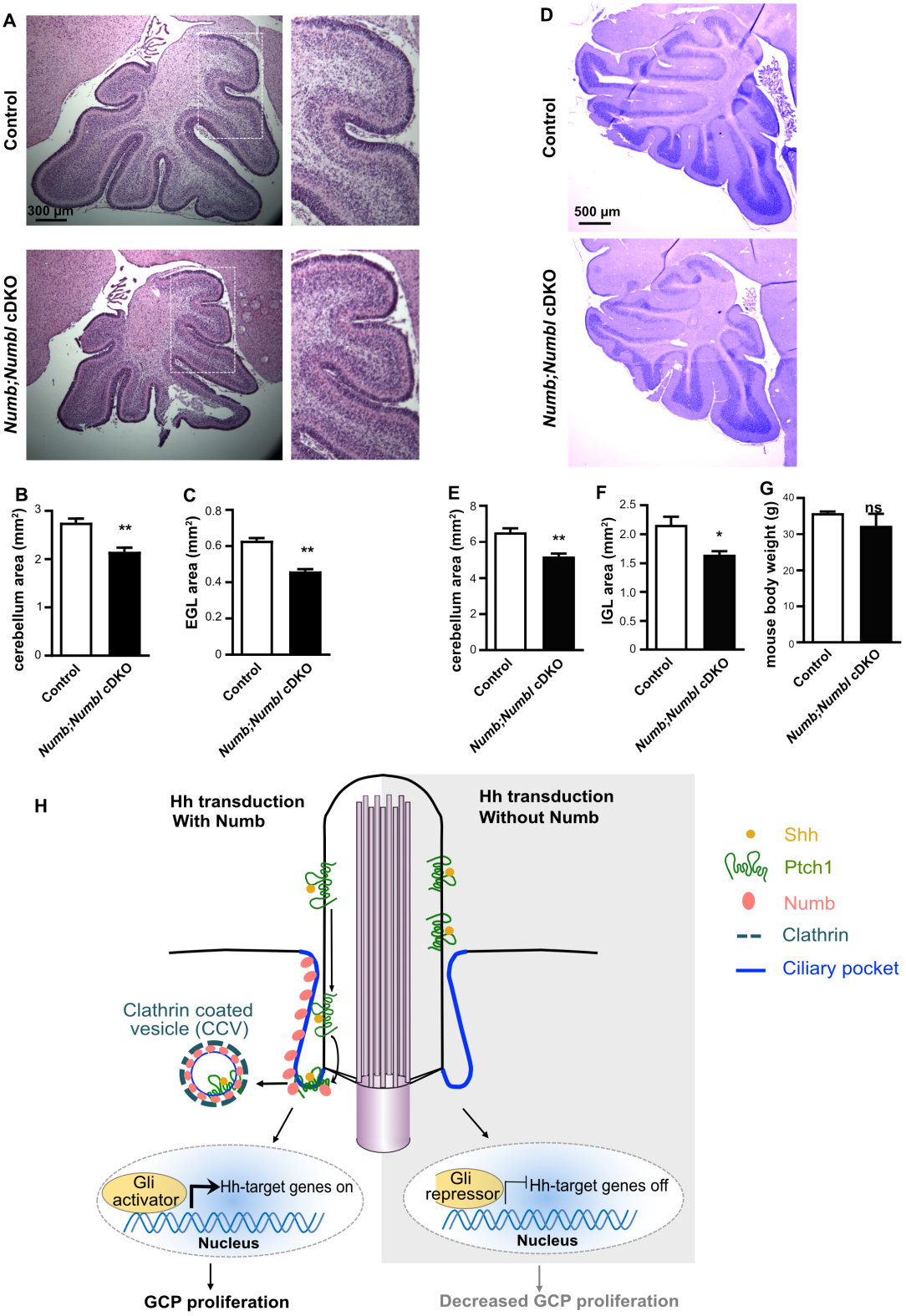

Figure 8. *Numb/Numbl* cDKO mice have a smaller GCP population and cerebellar size.
(A) Sagittal sections of cerebellum from P6 control and *Numb;Numbl* cDKO mice, stained with Hematoxylin and eosin (H & E). Boxes indicate the zoomed regions.

(B) Quantification of the overall cerebellar area (±s.e.m.) and **(C)** EGL area (±s.e.m.) in P6 mice measured at the same mediolateral level. n = 3 cerebella per group. Deletion of *Numb* and *Numbl* results in a smaller cerebellar areaand EGL area compared to control.
(D) Sagittal sections of cerebellum from adult control and *Numb;Numbl* cDKO mice with H & E staining.
(E) Quantification of the overall cerebellar area (±s.e.m.) and **(F)** IGL area (±s.e.m.) in the adult mice measured at the same mediolateral level. n = 3 cerebella per group. Deletion of *Numb* and *Numbl* results in a smaller cerebellar area and IGL area compared to control.
(G) Mean (±s.e.m.) adult mice body weight. n = 3 mice per group. Student's t-test, * = $p<0.05$, ** = $p<0.01$.
(H) Schematic of Numb's role in the cilium during activation of Hh signaling. Numb proteins at the ciliary pocket (blue lines) recruit Ptch1 into clathrin-coated vesicles thereby promoting Ptch1 exit from the cilium. This enables the maximal activation of Hh signaling, which sustains cell proliferation in tissues such as the developing cerebellum. Without Numb, Ptch1 remains in the cilium even after it binds to Shh. This subsequently compromises the maximal activation of the downstream signaling events, leading to attenuated target gene transcription in the nucleus and reduced Hh-dependent cell proliferation.

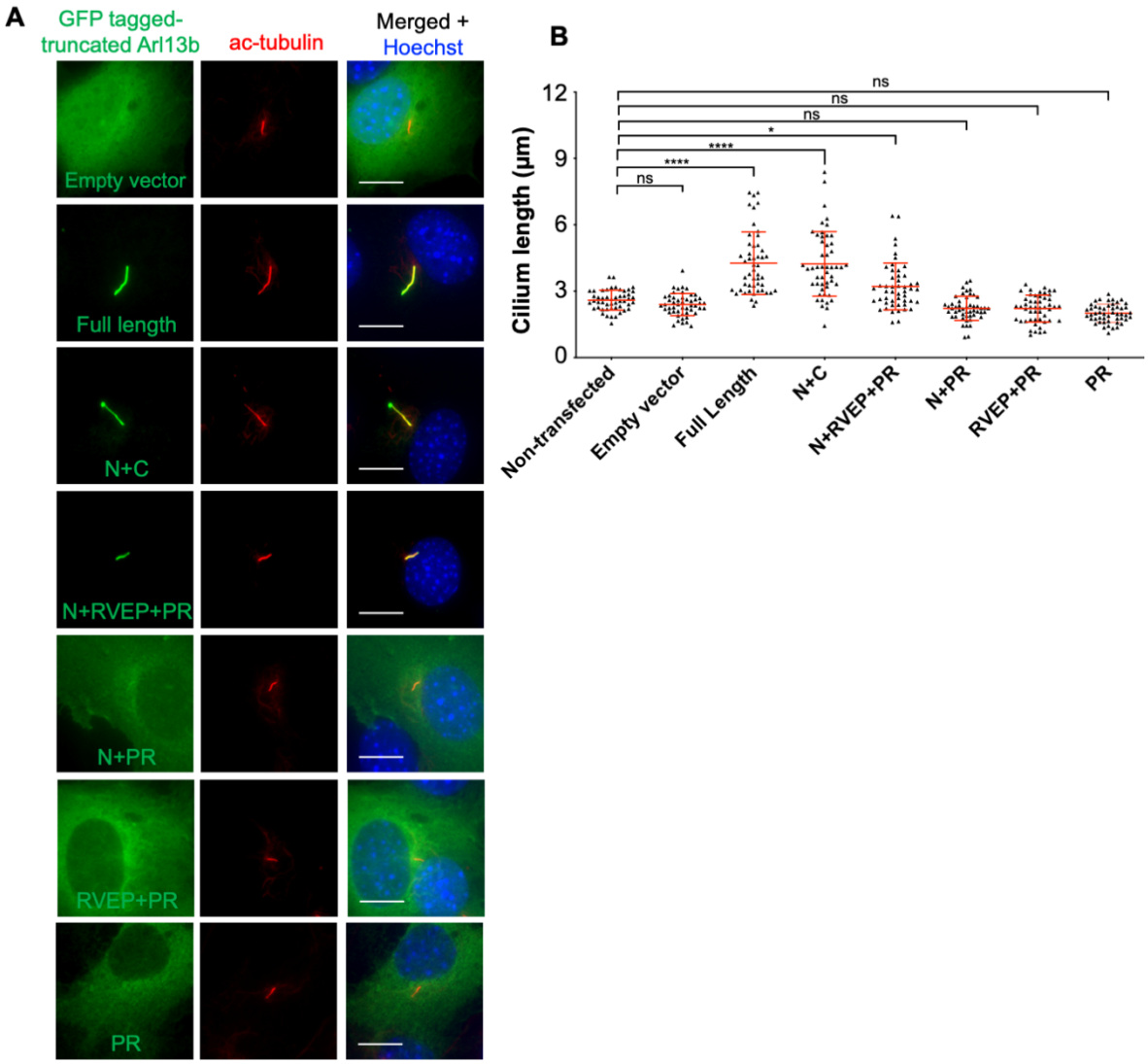

Figure S1. Truncated Arl13b localizes to the cilium with minimal impact on cilium length in transiently transfected cells.

(**A**) GFP-tagged truncated Arl13b constructs were transiently expressed in NIH3T3 cells. Cells were immunostained with an antibody against GFP and the cilium marker acetylated-tubulin. Scale bar, 10 µm.

(**B**) Quantification of the cilium length in cells transiently transfected with truncated Arl13b constructs. Note that in stable cell lines in Fig S2A where the expression levels are much lower, N+RVEP+PR has no significant impact on cilium length.

Data are shown as mean ± SD. n = 60 cilia per condition. One-way ANOVA with multiple comparisons (Tukey test). ****, $p < 0.0001$; *, $p < 0.05$; ns, not significant. Scale bars, 10 µm in all panels.

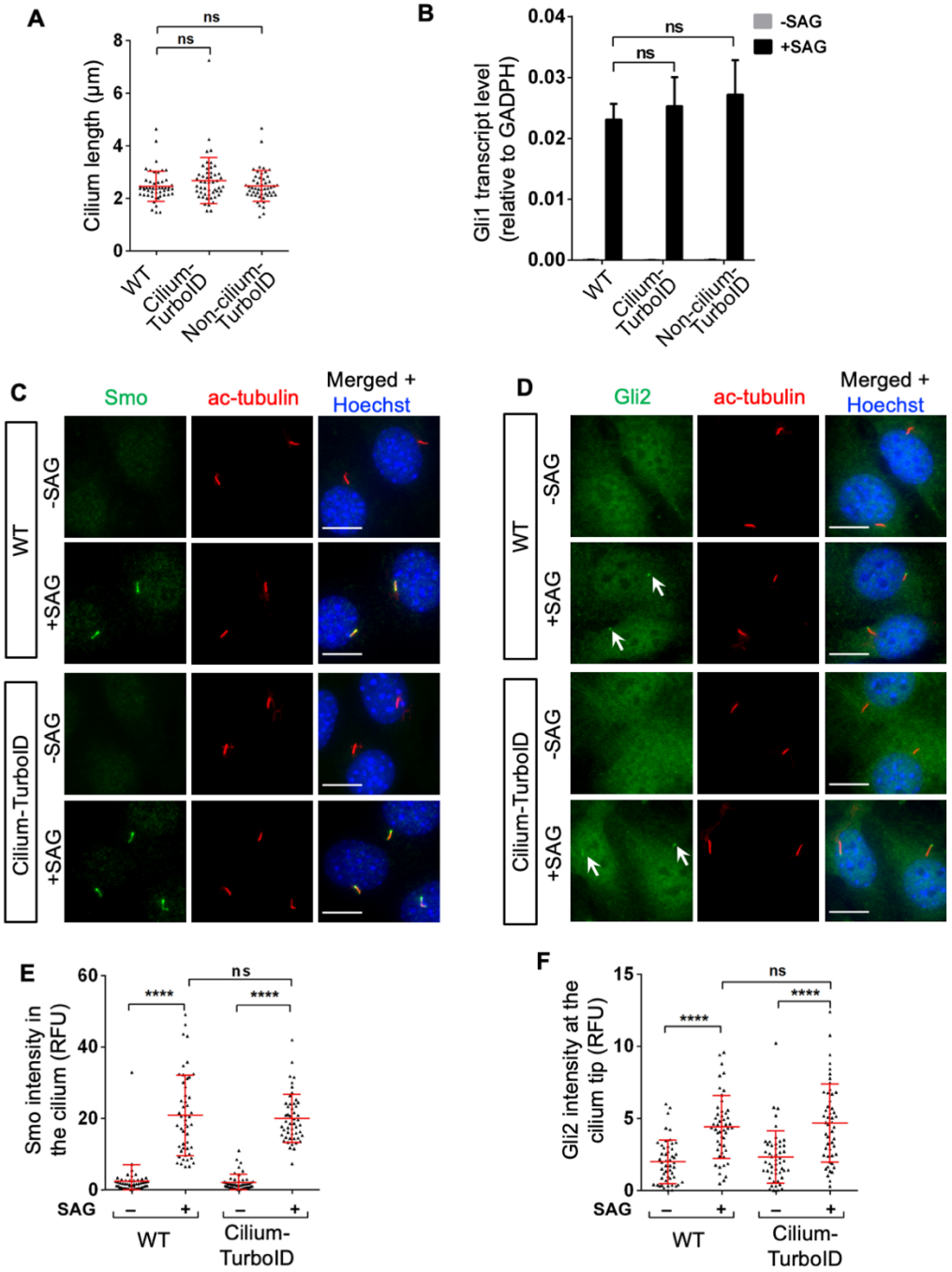

Figure S2. Cilium-TurboID in stable cell lines does not impact cilium morphology and Hh signal transduction.

(**A**) Quantification of the cilium length in WT (parental untransfected NIH3T3 cells), Cilium-TurboID and Non-cilium-TurboID stable cell lines. n = 50 cilia per condition.

(**B**) Cells were stimulated with SAG for 24h, and Hh signaling activity was evaluated by qPCR measuring *Gli1* transcript levels. Data are shown as relative transcript levels normalized to *GAPDH* (n = 4).

(**C-D**) Immunofluorescence of Smo and Gli2 in WT and Cilium-TurboID stable cell lines. Cells were serum-starved with or without SAG in the culture medium for 24 h. Arrows in (**D**) point to Gli2 fluorescence signal at cilia.
(**E-F**) Quantification of Smo and Gli2 fluorescence intensity in the cilium. Data are shown as mean ± SD. n = 50 cilia were quantified per condition. RFU, relative fluorescence unit.
Statistics: (**A**): one-way ANOVA with multiple comparisons (Tukey test). (**B, E** and **F**): two-way ANOVA with multiple comparisons (Tukey test), ****, $p < 0.0001$. All error bars represent SD; ns, not significant. Scale bars, 10 μm in all panels.

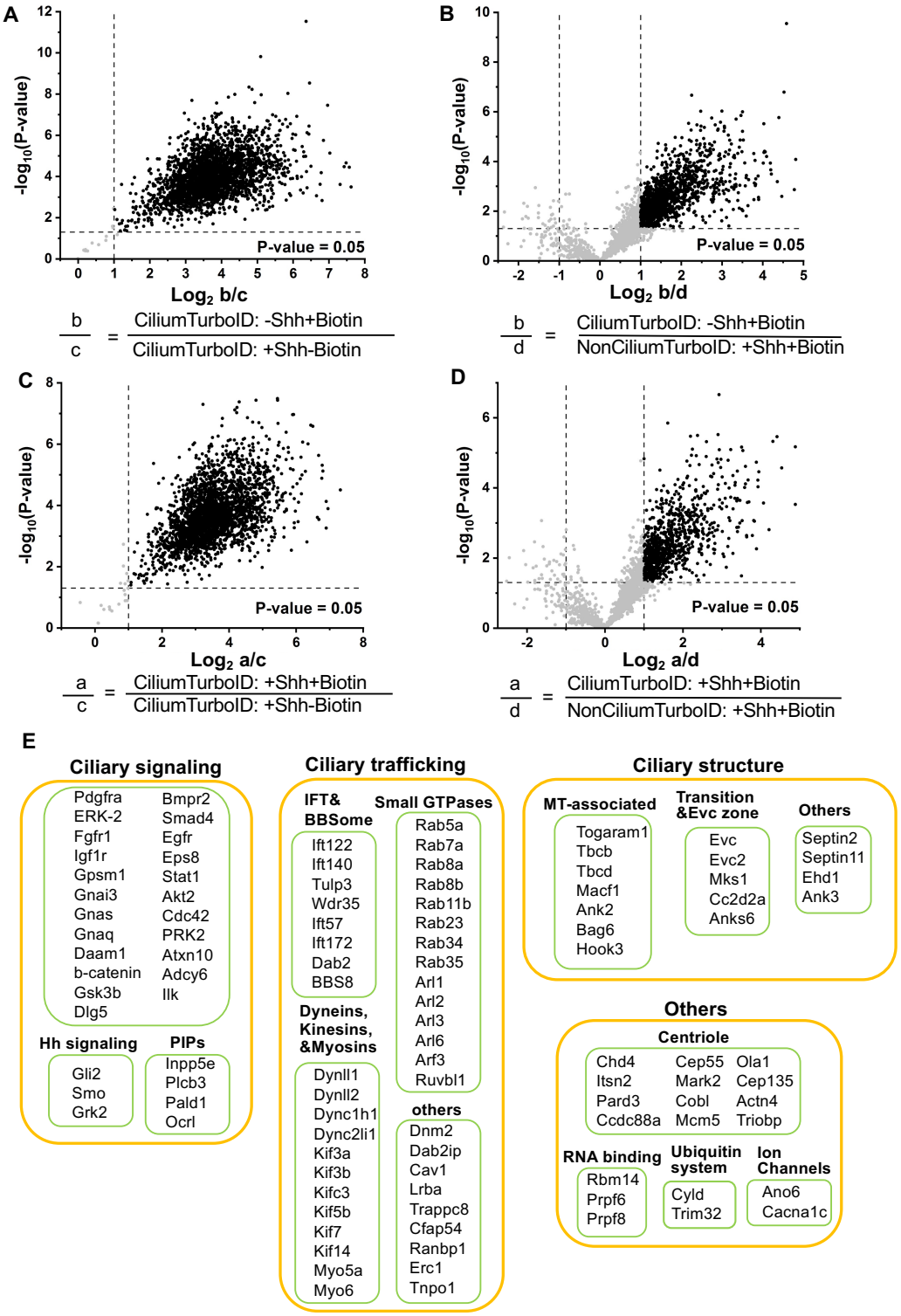

Figure S3. Identification of ciliary protein candidates from mass spectrometry.
Analysis was performed on 2,880 proteins that have more than 7 unique peptides. Volcano plots were generated by plotting the log2 TMT ratio of the indicated conditions against the negative log10 p-value of Student's t-test of the corresponding conditions. In each plot, dashed lines

indicate the cutoffs of $p < 0.05$ and TMT ratio > 2 or -2. Proteins that meet the cutoffs are represented by black dots. The proteins that meet the cutoffs were further analyzed as follows.
(1) The intersection of proteins in A (2643 candidates) and in B (1225 candidates) are defined as ciliary proteins without Shh stimulation; 788 proteins are identified in this category (Table S1).
(2) The intersection of proteins in C (2636 candidates) and in D (890 candidates) are defined as ciliary proteins with Shh stimulation; 574 proteins are identified in this category (Table S1).
(3) The union of candidates identified in step (1) and (2) are defined as ciliary candidates. 800 proteins are identified in this category (Table S2). These 800 proteins are plotted in Fig. 2C and Fig. 2E.
(**E**) The previously reported ciliary candidates recovered in this study are listed and grouped into functional categories.

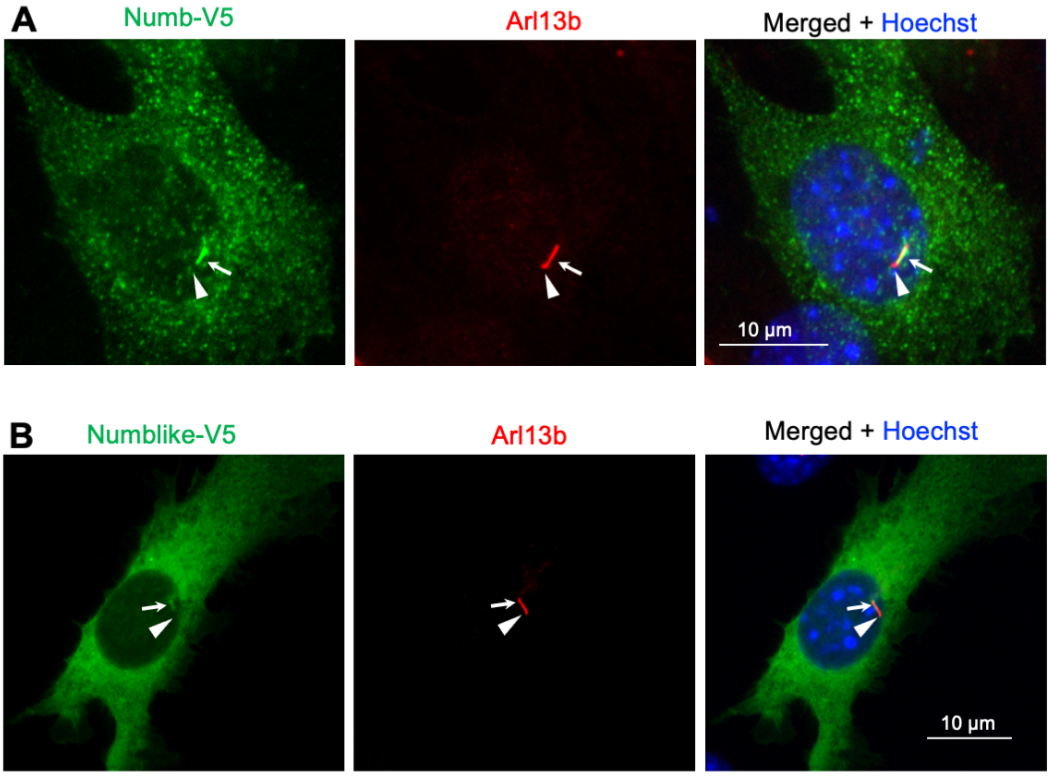

Figure S4. Numb and Numblike localize to the bottom segment of the primary cilium. Numb-V5 (**A**) or Numblike-V5 (**B**) were expressed in NIH3T3 cells and co-immunostained with the cilium marker Arl13b. V5 immunostaining overlaps with Arl13b at the lower segment of the cilium. White arrows point to the lower segment of the cilium where Numb and Numblike overlap with Arl13b; white triangles point to the tip of the cilium where no Numb or Numblike immunofluorescence signals are found.

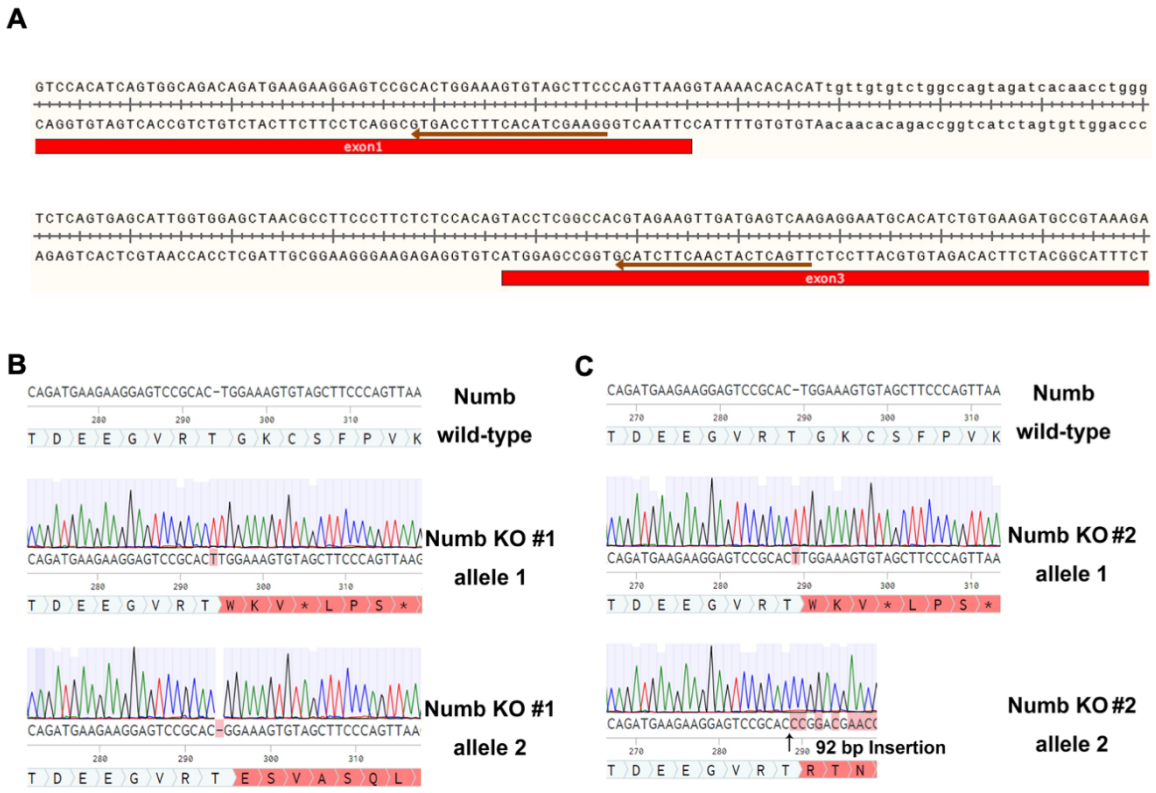

Figure S5. Design of Numb CRISPR/Cas9 and identification of genomic mutations in individual cell clones.

(**A**) Two guide RNAs were designed to target exon 1 and 3 of mouse *Numb*. Brown arrows indicate the sequence of gRNAs.

(**B-C**) The gRNA targeting region in the mouse genome was amplified by genomic PCR, ligated into TOPO vector, and transfected into chemically competent cells. 20 bacterial colonies of each cell clones were randomly picked and sequenced. The sequences are aligned with the Numb WT gene sequence from *M. musculus*. In Numb KO cell clone #1, a single-base-pair insertion and single-base-pair deletion were present. In Numb KO cell clone #2, a single-base-pair insertion and 92bp insertion were present. All mutations cause biallelic frameshift mutations that eventually lead to nonsense-mediated decay (NMD) of the mutant mRNA.

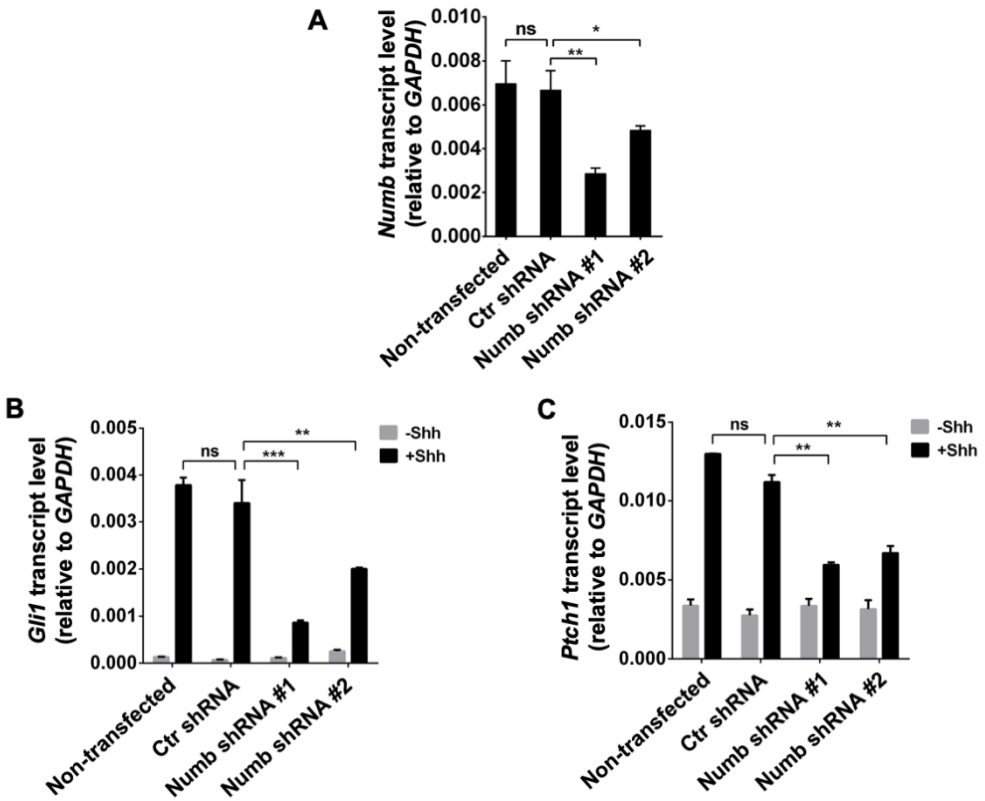

Figure S6. Numb shRNA impairs activation of Hh signaling.

(**A**) *Numb* shRNA significantly reduced *Numb* gene expression. *Numb* mRNA levels were measured by qPCR. Control (Ctr) shRNA is a non-mammalian targeting shRNA.

(**B-C**) 3 days after lentivirus-mediated transfection of *Numb* shRNA, cells were serum-starved for 24 h with or without Shh. Hh signaling activity was evaluated via qPCR measuring transcript levels of *Gli1* and *Ptch1*. *Numb* knockdown reduced Shh-induced Hh target gene transcription.

(**A-C**): one-way ANOVA with multiple comparisons (Tukey test). All error bars represent SD, n=3. ***, $p < 0.001$; **, $p < 0.01$; *, $p < 0.05$. ns, not significant.

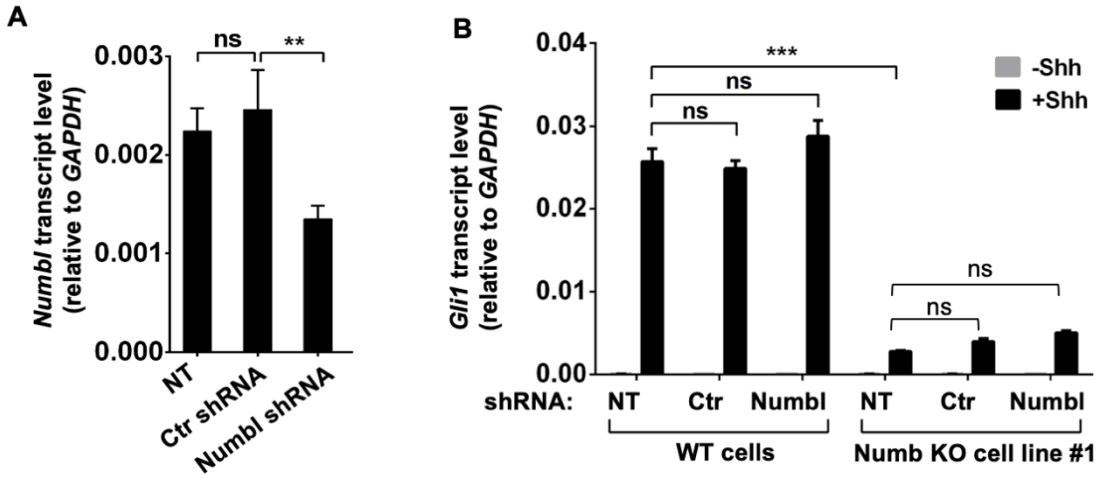

Figure S7. Knockdown of *Numbl* does not exacerbate Hh signaling defects in *Numb* KO cells.

(**A**) *Numbl* shRNA significantly reduced *Numbl* gene expression in NIH3T3 cells. *Numbl* mRNA levels were measured by qPCR.

(**B**) Parental (WT) NIH3T3 cells or *Numb* KO cells were infected with lentiviruses that express *Numbl* shRNA. 3 days after infection, cells were serum-starved for 24 h with or without Shh. Hh signaling activity was evaluated via qPCR measuring the transcript levels of *Gli1*. *Numbl* knockdown does not further reduce *Gli1* levels in *Numb* KO cells. Control (Ctr) shRNA is a non-mammalian targeting shRNA. NT: non-transfected.

(**A**): one-way ANOVA with multiple comparisons (Tukey test). (**B**): two-way ANOVA with multiple comparisons (Tukey test). All error bars represent SD, n=3. ***, $p < 0.001$; **, $p < 0.01$. ns, not significant. Scale bar, 10 μm.

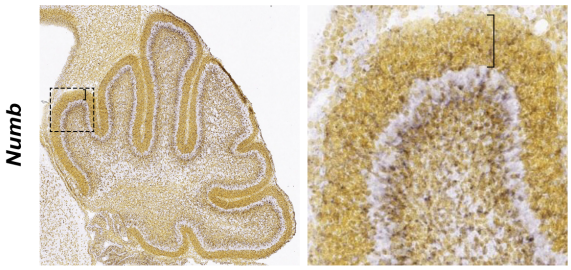

Figure S8. In situ hybridization for *Numb* mRNA in the developing cerebellum.
In situ hybridization on sagittal mouse sections at P4 for *Numb*. *Numb* mRNA is present in the EGL, Purkinje cells, and IGL. Bracket denotes the EGL. Box indicates zoomed area. Images obtained from The Allen Brain Atlas.